Frequent but Predictable Droughts in East Africa Driven By A Walker Circulation Intensification

Chris Funk[1], Andreas H. Fink[2], Laura Harrison[1], Zewdu Segele[3], Hussen S. Endris[3], Gideon Galu[1], Sharon Nicholson[4], Diriba Korecha[1]

[1]Climate Hazards Center, University of California, Santa Barbara

[2] Institute of Meteorology and Climate Research, Karlsruhe Institute of Technology, Karlsruhe, Germany

[3]IGAD Climate Prediction and Applications Center, Kenya

[4]Meteorology and Environmental Science, Florida State University

Corresponding Author: Chris Funk
Email: chrisfunk@ucsb.edu

Key Points:

- Human-induced warming in the western V area of the Pacific combined with La Niña, has produced frequent, predictable March-April-May droughts.
- Thermodynamic analyses link these droughts to a stronger Walker Ciruclation, driven by predictable warming in the Western V region.
- CMIP6 simulations indicate that western V warming is largely human-induced, this warming has enhanced and will enhance the Walker Circulation.

Abstract

The decline of the eastern East African (EA) March-April-May (MAM) rains poses a life-threatening 'enigma', an enigma linked to sequential droughts in the most food insecure region in the world. The MAM 2022 drought was the driest on record, preceded by three poor rainy seasons, and followed by widespread starvation. Connecting these droughts is an interaction between La Niña and climate change, an interaction that provides exciting opportunities for long lead prediction and proactive disaster risk management. Using observations, reanalyses, and climate change simulations, we show here, for the first time, that post-1997 OND La Niña events are robust precursors of: (1) strong MAM 'Western V Gradients' in the Pacific, which help produce (2) large increases in moisture convergence and atmospheric heating near Indonesia, which appear associated with (3) regional shifts in moisture transports and vertical velocities, which (4) help explain more frequent dry EA rainy seasons. Understanding this causal chain will help make long-lead forecasts more actionable. Increased Warm Pool atmospheric heating and moisture convergence sets the stage for dangerous sequential droughts in EA. At 20-yr time scales, we show that these Warm Pool heating increases are attributable to observed Western V warming, which is in turn largely attributable to climate change. As energy builds up in the oceans and atmosphere, we see stronger convergence patterns, which offer opportunities for prediction. Hence, linking EA drying to a stronger Walker Circulation can help explain the 'enigma' while underscoring the predictable risks associated with recent La Niña events.

Plain Language Summary

In 2022, an unprecedented sequence of five sequential droughts, exacerbated by high global food and fuel prices, drove an exceptional food security crisis in Ethiopia, Somalia and Kenya, pushing more than 20 million people into a food security crisis. Potential famine loomed in some areas. Beginning in late 2020, this was the longest and most severe drought recorded in the Horn in at least 70 years, resulting in multiple failed harvests and large-scale livestock deaths that decimated food and income sources for rural communities, placed increasing pressure on the cost of food among urban communities, and led to rising levels of destitution and displacement. These droughts occur against the backdrop of the 'East Africa Climate Paradox', which centers on the discrepancy between climate change model projections of increased East African March-April-May rains, and many observational studies pointing towards declines. Here, we show how framing this dilemma as an 'enigma' opens the door to explaining and predicting sequential East African droughts. The enigma we explore is 'why are so many recent La Niña events associated with dry March-April-May rains'? La Niña events tend to reach their maximum intensity in the boreal fall, often producing East African droughts. Before the western Pacific ocean warmed dramatically in 1998, the link between La Niña events and dry March-April-May rains was weak. Since 1998, the link is very strong. This sets the stage for dangerous sequential droughts, such as in 2010/11, 2016/17, 2020/21, 2021/2022, and perhaps 2022/23. We explain this enigma using observations, reanalyses, and the latest (Phase 6) climate change simulations.

While climate change models do recreate the observed East African drying, they do recreate very well the observed west Pacific warming. Climate change, not natural decadal variability associated with the Pacfic Decadal Oscillation, has increased west Pacific sea surface temperatures. This, in turn, is increasing the 'Western V Gradient', a measure of the east-west differences in Pacific ocean temperatures. When this gradient is negative, there are frequent East

African droughts, and this happens in a very predictable way during or after recent La Niña events. This allows us to predict many dry rainy seasons ~eight months in advance. Such predictive capacity is important, because the frequency of strong Pacific temperature gradients is increasing, and we shown that climate change simulations recreate this tendency, and expect it to increase over the coming decades.

What connects East African droughts to Pacific temperature gradients? We answer this question by examining observed atmospheric heating, moisture transports, and moisture convergence patterns. In general, eastern East Africa is dry because it resides along the western edge of the Indian Ocean branch of the Indo-Pacific 'Walker Circulation'. Across East Africa and the western Indian Ocean, and over the central and eastern Pacific, rainfall and moisture levels are low. In the area around Indonesia (the eastern Indian and western Pacific Oceans), winds drive moisture convergence and heavy rains. Here, building on many years of research by scientists working for the Famine Early Warning Systems Network, we show for the first time that the strength of the Walker Circulation can be quantified using atmospheric heating and moisture convergence. When heating and moisture convergence is high in the area around Indonesia, East African rains are almost always dry. Since 1998, when there has been a La Niña in October-November-December, there has almost always been strong March-April-May heating and moisture convergence around Indonesia. This resolves the enigma. Climate change-enhanced La Niñas amplify the Pacific trade winds, producing strong March-April-May sea surface temperature gradients, which amplify the Walker Circulation, which reduce moisture convergence and ascending atmospheric motions over the eastern Horn of Africa.

We conclude with a look toward the future evolution of the Walker Circulation, by relating the observed strength of the Walker Circulation to 20-yr averages of western and eastern Pacific sea surface tempertures. Both play a significant role, and together explain 96% of the observed variability. The observed Walker Circulation intensification is primarily driven by the west Pacific, which in turn is strongly related to climate change. CMIP6 projections of Pacific sea surface temperatures, combined with the observed empirical relationships, imply further strong increases in Walker Circulation intensities. Hence, further rainfall declines appear likely, especially before or after La Niña events. But the process-based analyses presented here suggests that many of the dry seasons may be predictable, based on Pacific sea surface temperature gradients.

1 Introduction – CMIP6 simulations can enhance drought early warning to support food security

This study examines the drivers of March-April-May rains in eastern East Africa (EA), a region of extreme food insecurity and frequent droughts[*Shukla et al.*, 2021]. Located near the equator and the descending branch of the Indian Ocean branch of east-west Walker Circulation, this region receives rains in OND and MAM [*Brant Liebmann et al.*, 2012; *Nicholson*, 2017]. Sequential OND/MAM droughts can have profound food security impacts, as in 2010/2011, when more 250,000 Somalis perished due to famine[*Checchi and Robinson*, 2013]. In 2020-2022 an unprecedented sequence of five dry seasons, associated with a three-year La Niña event, led to a massive humanitarian crisis, potential famine, and widespread loss of livestock and livelihoods [*ICPAC et al.*, 2022a; *ICPAC et al.*, 2022b]. These crises occur amidst a continuing and well-documented decline in MAM 'long' rains, as first identified by the Famine Early Warning Systems Network (FEWS NET) [*Funk et al.*, 2005; *Verdin et al.*, 2005], and later studies [*Lyon*, 2014; *Lyon and DeWitt*, 2012; *Yang et al.*, 2014]. Following the 1997/98 El Niño, dry MAM seasons became more frequent [*Lyon*, 2014], while the variability of OND rains increased [*Nicholson*, 2015]. The MAM season is also becoming 'shorter not less intense' due to regional circulation changes [*Wainwright et al.*, 2019].

Our focus here is the potential link between climate change and the dramatic post-1998 increase in the frequency of dry MAM seasons, following OND La Niñas. This increase sets the stage for dangerous OND/MAM multi-season droughts [*Funk et al.*, 2018], but also opens opportunities for predicting the MAM rains, as in 2017 [*Voosen*, 2020] and 2021 and 2022[*Rubiano*, 2022]. As noted in a 2022 multi-agency alert [*ICPAC et al.*, 2022a], between 1950 and 1997, OND La Niña conditions, as defined by the Climate Prediction Center[*NOAA*, 2022], did not alter the odds of a below-normal (bottom tercile) EA MAM rainy season. Following the twelve La Niñas since OND 1998, nine rainy seasons have been poor. This shift, and OND La Niña conditions in 2020, 2021, and 2022 has contributed to repetitive droughts and potential famine conditions in 2023[*ICPAC et al.*, 2022b]. Here, in contrast with other valuable studies that focused on larger domains, regional climate processes, or sub-seasonal drivers [*Finney et al.*, 2020; *Nicholson*, 2017; *Wainwright et al.*, 2019], we focus here on large-scale teleconnections that may help identify, explain and predict recent below-normal EA MAM rainy seasons. These results help explain regional circulation changes consistent with a 'shorter not less intense' rainy season [*Wainwright et al.*, 2019] and the increasing links to the El Niño Southern Oscillation (ENSO) [*Park et al.*, 2020]. Our goal in this paper is to support early warning and forecasting efforts by explaining the links between La Niña, predictable Pacific SST gradients and EA dry seasons, on both interannual and decadal time-scales.

Our study proceeds in three stages. We first examine CMIP6 and observed EA MAM precipitation and Pacific sea surface temperatures (SST). This links EA drying to human-induced warming in the west Pacific. Then, using reanalyses, we show that strong Pacific SST gradients and Walker Circulation disruptions follow post-1997 La Niñas. Seasons with more intense with Walker Circulations are clearly linked to a preponderance of dry EA MAM seasons. We then use observed Pacific SST gradients and CMIP6 SST projections to suggest that human-induced west

Pacific warming has, and will, enhance the Walker Circulation in ways associated with drying over EA.

1.1 Background – Describing the 'East Africa Enigma'

Following its introduction in 2015 [*Rowell et al.*, 2015], several papers have discussed the 'East African Climate Paradox' [*Lyon and Vigaud*, 2017; *Wainwright et al.*, 2019] – while observations clearly indicate more frequent dry seasons along with later starts and early cessation [*Wainwright et al.*, 2019], climate change simulations have indicated rainfall increases. While natural Pacific Decadal Variability (PDV) [*Lyon*, 2014; *Lyon and Vigaud*, 2017; *Yang et al.*, 2014] might explain this change, it is becoming more and more likely that the 'paradox' arises due to the models' systematic biases in SSTs and African circulation features [*Lyon*, 2020; 2021; *Schwarzwald et al.*, 2022; *Shukla et al.*, 2016; *J E Tierney et al.*, 2015]. The terrain and teleconnections controlling precipitation in EA are complex and poorly resolved by global climate models [*Endris et al.*, 2016]. The models tend to misrepresent the mean zonal SST gradients in the Indian Ocean [*Lyon*, 2021; *Lyon and Vigaud*, 2017; *Schwarzwald et al.*, 2022] and Pacific Ocean [*Seager et al.*, 2022; *Seager et al.*, 2019]. Over EA they tend to have a seasonal cycle that is far too wet in OND and dry in MAM [*J Tierney et al.*, 2013]. Multi-model ensembles of regional climate model simulations perform much better [*Endris et al.*, 2013], and indicate decreased rainfall in MAM [*Ogega et al.*, 2020]. Recent evaluations of regional and global climate change models [*Endris et al.*, 2019] indicate stronger future ENSO teleconnections during MAM, consistent with several climate change studies indicating an increased frequency of strong-gradient La Niñas [*Cai et al.*, 2022; *Cai et al.*, 2015b].

In place of the 'paradox', we focus here on the 'East African Climate Enigma'. The 'enigma' relates the increased frequency of dry MAM seasons, following OND La Niñas, to predictable 'Western V' SST gradients (described below) in MAM. The Western V region begins in equatorial West Pacific (near Indonesia), and extends poleward into the extra-tropical northern and southern Pacific. Warm SSTs in this region have been linked to dry EEA MAM rainy seasons [*Funk et al.*, 2018; *Funk et al.*, 2019] and the West Pacific Warming Mode [*Funk and Hoell*, 2015]. From a food security perspective, the link between OND La Niñas and MAM rainfall deficits is important, because it sets the stage for dangerous sequential droughts. Long lead MAM rainfall forecasts have helped guide humanitarian responses in 2017 [*Voosen*, 2020], and 2021/2022 [*Button*, 2022]. But while they are effective, there has not been relatively little research focused on how strong Pacific SST gradients induce dry EA rainy seasons, why such conditions tend to be associated with La Niña events, and how human-induced warming might be influencing outcomes.

2 Methods

The focus here will be on explaining the link between recent (post-1997) OND La Niñas, as defined by OND[*Funk et al.*, 2018; *Funk et al.*, 2019] NOAA Oceanic Niño Index, ONI values [*NOAA*, 2022] and frequent MAM dry seasons in the following year. This also relates to recent work documenting increasing ENSO-East Africa teleconnections [*Park et al.*, 2020]. While forecasting is not the focus here, these explorations provide process-based insights that can inform operational forecasts, such as those provided by the IGAD Climate Prediction and

Aplications Center (ICPAC, www.icpac.net) or the Climate Hazards Center (CHC, blog.chc.ucsb.edu). Our goals are to better understand links between the WVG and La Niñas, the WVG and the Walker Circulation, and the WVG and climate change. This work has implications for seasonal climate prediction, humanitarian assistance programming, and climate change adaptation. Our study progresses in three stages.

2.1 Linking droughts to predictable Pacific SST gradients and human-induced warming in the west Pacific

We begin by describing the 'East African Climate Paradox' [*Rowell et al.*, 2015] using updated (through 20220 rainfall and SST observations and CMIP6 precipitation simulations. Composites of SSTs for dry and wet seasons are evaluated. Dry events, but not wet events, are associated with coherent SST teleconnections. Dry MAM seasons are characterized by very warm west Pacific 'Western V' SSTs. The western V originates in the Warm Pool area around Indonesia and extends northeast and southeast into the extra-tropics. Warm Western V conditions have been linked to recent MAM droughts [*Funk et al.*, 2018; *Funk et al.*, 2019]. Warming in this region also loads heavily on the 'West Pacific Warming Mode', the first empirical orthogonal function of global ENSO-residual SST [*Funk and Hoell*, 2015]. We define the 'Western V Gradient' (WVG) as the difference between standardized NINO3.4 and Western V SSTs. Since the west Pacific warmed following the 1997/1998 El Niño [*Lyon et al.*, 2013] and the Walker Circulation intensified [*L'Heureux et al.*, 2013], OND La Niña events [*NOAA*, 2022] are always followed by strong negative WVG values in MAM. We show that these WVG values are very predictable. We also show that these predictions do a good job of indentifying many dry MAM seasons at long leads. Using observations, we show that since 1999, strong negative MAM WVG events always follow La Niña events in the previous OND, when the La Niña signal tends to be at its peak. Then, using CMIP6 simulations, we examine the level of correspondence between the simulated SST warming trends, and observed outcomes in the NINO3.4 and Western V regions, as well as the WVG.

2.2 Linking La Niña/WVG events to Walker Circulation Intensification

This section examines interannual WVG influences on MAM Indo-Pacific atmospheric heating, moisture transports, and moisture convergence fields. Long term means and WVG anomalies in atmospheric heating and moisture transports can be used to explore the Indian and Pacific branches of the Walker Circulation [*Bjerknes*, 1969]. Note that we use the term 'Walker Circulation' to broadly refer to the complex Indo-Pacific circulation patterns linking the Pacific to the Warm Pool region near Indonesia, and the Warm Pool region to MAM EA rains. While we present equatorial longitude-by-height results, we also examine spatial maps which emphasize that emphasize how extra-tropical SST and atmosopheric heating gradients act to modulate moisture transports.

Our thermodynamic approach was inspired by studies using vertically integrated transports of heat energy (internal energy, T) and geopotential height energy (potential energy, Z) [*Peixoto and Oort*, 1992; *Trenberth and Stepaniak*, 2003a; b]. T is a function of the vertical temperature distribution and specific heat capacity of air, Z is a function of geopotential height and g, the acceleration due to gravity. These are the two largest atmospheric energy terms. In atmospheric

thermodynamics, it is common to combine these two terms to describe changes in Dry Static Energy (DSE):

$$DSE = T + Z \quad \text{eq. 1}$$

DSE is a conserved quantity. Changes in DSE, however, arise from the introduction of external heating, commonly referred to as diabatic heating. Latent heating (LH) due to precipitation, radiation (R), and sensible heating (SH) in the planetary boundary layer are the largest sources of diabatic heating. The R term here is a measure of the net radiation into a column of air, i.e. a combination of the downward and upward shortwave radiation from the top of the atmosphere and surface of the Earth. Increased atmospheric water vapor contributes to increased trapped longwave radiation and increased precipitation. As the atmosphere warms and saturation vapor pressures increase, these heating terms are likely to increase as well. DSE is a conserved quantity, modulated by external (diabatic) heating, which leads to:

$$\text{diabatic heating} = Div(T) + Div(Z) \quad \text{eq. 2}$$

Where Div(T) and Div(Z) are vertically-integrated divergence terms, based on vertically integrated temperature and geopotential height fluxes. While accurate, the standard DSE formulation of these terms obscures the fact that Div(T) and Div(Z) are strongly anti-correlated, due to hydrostatic relationships [*Peixoto and Oort*, 1992]. Converging heat in the lower and middle troposphere causes a column of air to stretch, raising upper-level heights, and increasing Div(Z). In rainy areas of the Walker Circulation, heat converges in the lower troposphere, and geopotential height energy diverges aloft. Persistent heating in the Indo-Pacific Warm Pool area produces equatorially-trapped Rossby and Kelvin waves, which (respectively) help establish the Indian and Pacific branches of the Walker Circulation [*Gill*, 1980; 1982]. To measure the strength of this forcing, we combine diabatic heating and heat convergence into a single 'atmospheric heating' term, measured in Wm^{-2}.

$$\text{atmosperhic heating} = Con(T) + \text{diabatic forcing} \quad \text{eq. 3}$$

As we will show, this framework provides a useful description of the humid and dry regions of the Walker Circulation. Areas with low level convergent winds will have both heat convergence Con(T) and moisture convergence Con(Q). Direct heating by heat convergence will be augmented by latent heat released via precipitation, since moisture is also conserved:

$$\text{precipitation} = Con(Q) - \text{evaporation} \quad \text{eq. 4}$$

Since evaporation in Warm Pool areas tends to be low, precipitation ≈ Con(Q). More moisture will also increase the trapping of longwave radiation. Eq. 3, therefore, stacks covarying heating terms. From first principles, a warming atmosphere might experience increased heat convergence, simply due to increases in air temperatures, as well as increases in precipitation and decreases in outgoing longwave radiation, due to increased atmospheric water vapor. This logic also supports combining these heating terms. We examine these variables to formally evaluate whether a Walker Circulation enhancement is linked to dry EA rainy seasons. Contrasting these fields, in MAM seasons following 1998-2021 OND La Niñas and 1950-1997 La Niñas helps

explain links between distant WVG SST patterns and local reductions in EA MAM total precipitable water, vertical ascent, and precipitation. Changes in the Indian Ocean branch of the Walker Circulation alter moisture transports and intensify subsidence over the eastern Horn of Africa.

2.3 Linking Western V warming to Walker Circulation intensification and more frequent dry EA rainy seasons

Our final analysis focuses on decadal changes in the strength of the Walker Circulation and the frequency of below-normal MAM rainy seasons. We begin by updating the observational West Pacific Warming Mode (WPWM) analysis from Funk and Hoell (2015). This Empirical Orthoganal Function analysis underscores the points that 1) NINO3.4 and Western V and NINO3.4 SSTs closely track the first two modes of global SST, and 2) the climate-change-related WPWM, along with Western V SSTs, continues to increase rapidly. We then use regression to link 20-yr average Western V and NINO3.4 SST to 20-yr averages of Warm Pool atmospheric heating. We show that these SST values explain very well 20-yr changes in Warm Pool atmospheric heating and that the Western V warming has played an important role in the recent Walker Circulation intensification and the increased frequency of dry East African rainy seasons. CMIP6 SST ensembles are used to estimate increases in Warm Pool heating through 2050.

3 Data

Dry and wet seasons are defined using satellite-gauge [*Funk et al.*, 2015b] and interpolated gauge [*Funk et al.*, 2015a] datasets. These widely used data sets were specifically developed to work well in East Africa, work well [*Dinku et al.*, 2018], and incorporate many additional raingauge observations provided by collaborators at Florida State University [*Nicholson*, 2017], the Ethiopian Meteorological Agency (~120 stations), and the Somali Food Security and Nutrition Analysis Unit (~90 stations). The EA area of focus is based on the region used in a mid-2022 multi-agency alert focused on the failure of the MAM 2022 rains[*ICPAC et al.*, 2022a]. Areal averages of the 1981-2022 Climate Hazards InfraRed Precipitation with Stations (CHIRPS) [*Funk et al.*, 2015a] and the 1900-2014 Centennial Trends [*Funk et al.*, 2015b] correlate very well over their period of overlap (1981-2014). A bivariate regression is used to transform Centennial Trends values into CHIRPS-compatible regional averages over the 1950-1980 period. A Gamma distribution fit is then used to develop a Standardized Precipitation Index (SPI) times-series [*Husak et al.*, 2007]. This time series, and all other analyses in this study, are centered on a 1981-2021 baseline. Dry and wet seasons will be based on the EA SPI values below and above -0.44Z and +0.44Z, which corresponds with a 1-in-3 year low or high value. Dry seasons may occasionally be described as droughts, to avoid repetition. Version 5 of the NOAA Extended SST [*Huang et al.*, 2017] is used to represent ocean temperatures. To explore circulation changes we use ERA5 [*Hersbach et al.*, 2020] and MERRA2 [*Gelaro et al.*, 2017] reanalyses. Our analysis looks at moisture transports and the combined influence of local diabatic heating and atmospheric heat convergence. We also include in our study August

forecasts of MAM SSTs from the North American Multi-Model Ensemble (NMME)[*Kirtman et al.*, 2014].

Our study also uses a multi-model ensemble of 152 Shared Socio-Economic Pathway 245 SST simulations from the latest CMIP version 6 (CMIP6) archive [*Eyring et al.*, 2016] (Table 1). The moderate SSP245 scenario is based on projections of large increases in sustainable development and 4.5 Wm^{-2} of radiative forcing [*Meinshausen et al.*, 2020]. CMIP6 data were accessed from Lawrence Livermore National Laboratory (LLNL) node of the Earth System Grid Federation (ESGF) platform (https://esgf-node.llnl.gov/search/cmip6/).

Finally, it should be noted that most of our observational results focus on the 1981-2022 time period, during which satellite data informs our precipitation estimates and reanalyses. While we do present longer time-series of EA rainfall, and changes in 1950-2022 ERA5 WVG events, the bulk of our analysis focuses on the past 42 years. This allows for cross-checks between the ERA5 and MERRA2 reanalyses.

4 Results

4.1 Links between OND La Niña, predictable strong Western V Gradients and EA Droughts

In MAM 2022, rains in Ethiopia, Kenya and Somalia were exceptionally poor (Fig. 1A,B). Here, as in several previous FEWS NET [*Funk and al.*, 2019] studies [*Funk et al.*, 2014; *Funk et al.*, 2018; *Funk et al.*, 2019; *B. Liebmann et al.*, 2014], we focus on a specific spatial subset of the Greater Horn of Africa, eastern East Africa (purple polygon shown in Fig. 1A), not a broader region as in [*Finney et al.*, 2020; *Walker et al.*, 2020], because this extremely food insecure region [*Shukla et al.*, 2021] experiences frequent sequential droughts, especially during or following recent La Niña events [*Funk et al.*, 2014; *Funk et al.*, 2018; *Funk et al.*, 2019; *Hoell and Funk*, 2013a; b; *B. Liebmann et al.*, 2014; *Williams and Funk*, 2011]. Since 1999, 11 seasons have been dry. Many of these dry seasons have also followed 12 post-1997 OND La Niñas (yellow circles, Fig. 1B). We refer to these events as 'Western V Gradient' events (described further below), because even if La Niña conditions fade, strong Pacific gradients, augmented by west Pacific warming, may be conducive to dry EA MAM outcomes [*Funk et al.*, 2018; *Funk et al.*, 2019].

The observed drying contrasts with results (Fig. 1C,D) from 152 CMIP6 SSP245 simulations (Table 1). Time-series of 30-yr average SPI indicate little change. The last observed and simulated values from this time-series (1993-2022 average SPI) are expanded in Fig. 1D, which breaks the results out by model. The observed 30-yr SPI value is very unlikely given the observed range of CMIP6 averages. This could be explained by a large natural internal decadal variation, potentially related to the Pacific (further discussed below), or it might relate to issues associated with poor representations of mean Indo-Pacific SSTs and EA seasonality and teleconnections (discussed above in section 1.1).

Composites of standardized MAM SSTs during 1981-2022 dry seasons (Fig. 2A) exhibit a contrast between a warm 'Western V' region in the west Pacific and cool central-east Pacific SSTs. Western V SST are averaged over the equatorial west Pacific (120-160°E, 15°S-20°N),

Western North Pacific (160°E-150°W, 20°N-35°N) and Western South Pacific (155°E-150°W, 15°S-30°S). Western V [*Funk et al.*, 2019] and Western North Pacific SST [*Funk et al.*, 2018] have been linked to dry EA rains, and FEWS NET uses a standardized gradient between NINO3.4 and Western V SSTs (the Western V Gradient, WVG) to inform operational long-lead predictions. Interestingly, while dry MAM season composites exhibit significant links to the Pacific (Fig. 2A), and some relation to Indian Ocean SSTs, wet season composites indicate less strong links (Fig. 2B). Non-linearities have been previously identified for the OND season [*Nicholson*, 2015], but have received little attention in MAM. Dry events may be more predictable than wet events.

Enigmatically, strong negative MAM WVG conditions are very common following recent OND La Niñas, and are also associated with many of the recent dry EA MAM seasons (Fig. 2C). There have been 12 OND La Niñas since 1998, and the MAM WVG values the following year ranged from -0.8Z to -2.2Z. Nine of these MAM seasons were dry EA years. Here, we will describe the 12 post-1997 MAM seasons that follow the last 12 La Niñas as 'WVG events'. It is important to differentiate these from La Niñas, because warm Western V SSTs can linger after a La Niña fades (as in 2016/17) producing La Niña-like impacts in MAM, consistent with stronger ENSO teleconnections [*Park et al.*, 2020]. Strong warming trends in the western Pacific [*Funk et al.*, 2018; *Funk et al.*, 2019] and frequent La Niñas since the late 1990s have led to a marked increase in the frequency of strong negative WVG conditions during MAM (Fig. 2C).

We can predict WVG conditions at long leads, allowing us to predict many of the events that produce the decline in EA rains. As an example, Fig. 2D shows forecasts of MAM WVG values, based on September North American Multi-Model Ensemble climate forecasts[1] [*Kirtman et al.*, 2014]. Western V, WVG and NINO3.4 SSTs are all predicted very well by the NMME (1982-2022 R^2 0.77, 0.77, 0.67). When WVG values are predicted to be negative (< -0.5Z) we see a preponderance of dry EA MAM rainy seasons, and many of the seasons with low WVG values follow OND La Niñas. The societal import of Fig. 2D is very important, because this approach can help anticipate dangerous OND/MAM sequential droughts, which in 2020-2022 brought four sequential dry seasons and the threat of starvation to millions in Ethiopia, Kenya, and Somalia [*ICPAC et al.*, 2022a].

Figure 3 presents observed and simulated changes in 20-yr MAM Western V, NINO3.4 and WVG time-series. For the Western V, the observations track very closely with the CMIP6 simulations (Fig. 3A). The correlation between the CMIP6 median Western V values and the observed Western V time-series is 0.96. The CMIP6 simulations suggest that climate change, not natural Pacific Decadal variability, has resulted in large SST increases in the western V region. The pace of observed warming has increased dramatically over the past 20 years. The observed 2003-2022 Western V average falls comfortably within the CMIP6 distribution (Fig. 3B). This contrasts with NINO3.4 outcomes (Fig. 3C-D). As noted by other studies, in observations, there is marked lack of warming in the eastern Pacific [*Seager et al.*, 2022; *Seager et al.*, 2019]. The CMIP6 ensemble, on the other hand, predicts substantial warming. The distribution of standardized 2003-2022 CMIP6 NINO3.4 values (Fig. 3D) suggests that the observed lack of cooling is very unlikely, given the simulations. This might arise due to an extreme expression of

[1] https://www.agrilinks.org/post/forecast-update-east-africa-likely-experience-six-droughts-row

natural decadal variability. However, it seems increasingly likely that systematic biases in Pacific SST may also contribute to this discrepancy [*Seager et al.*, 2022; *Seager et al.*, 2019].

As one would expect, WVG observations and CMIP6 simulations (Fig. 3E-F), fall between panels 3A-B and 3C-D. While the observed 2002-2023 WVG value (-0.5Z) falls at the edge of the CMIP6 distrubution (Fig. 3F), the CMIP6 ensemble does predict reductions in the WVG (Fig. 3E), due to the influence of human-induced warming in the Western V. Assuming that the CMIP6 WVG simulations are 'true', and that the lack of warming in the NINO3.4 region is natural, these results still indicate that about half of the observed increase in the WVG has been caused by climate change. If the CMIP6 models are over-estimating warming the NINO3.4 region, then climate change would account for a greater portion of the observed decrease in WVG values.

4.2 Linking WVG events to large and energetic changes in the Walker Circulation

A better understanding of the processes that link Pacific SSTs and dry EA outcomes will help build confidence in dry season outlooks, which will make them more actionable. To that end we examine MAM WVG circulation anomalies using ERA5 and MERRA2 reanalyses. As discussed in the methods section, atmospheric heating is inversely correlated with the divergence of geopotential height energy (Fig. 4A-B), and the long term mean atmospheric heating (Fig. 4C) and geopotential divergence fields (Fig. 4D) help delineate the low and high pressure cells that comprise the global Walker Circulation.

Climatologically, the atmospheric heating that drives the Walker Circulation can be visualized by examining maps of vertically integrated diabatic heating (Fig. 5A) and atmospheric heat convergence (Fig. 5B). These are the two terms on the right hand side of eq. 3. In the tropics, diabatic heating in the lower and middle troposphere destabilizes the atmosphere and produces lower surface pressures, which drives atmospheric heat convergence (Fig. 5B). We refer to the combination of diabatic heating and heat convergence as atmospheric heating. Because temperatures and water vapor are both larger in the lower troposphere, vertically integrated heat and moisture transports are very similar. Areas with strong moisture convergence will have heavy precipitation, and strong heat convergence, and large amounts of water vapor will trap longwave radiation. In the Indo-Pacific, this region is often referred to as the 'Warm Pool'. Fig. 5A,B also show long term average moisture transports. The Pacific Trade winds feed very large transports of heat and moisture into the Warm Pool, linking the Walker Circulation to Pacific SSTs.

In MAM, the Indian Ocean branch of the Walker Circulation can be characterized by strong atmospheric heating (>450Wm^{-2}) in the eastern equatorial Indian Ocean, and heat divergence (<-270 Wm^{-2}) over the southern and equatorial western Indian Ocean (Fig. 5AB). This strong heating gradient produces a strong low-level pressure gradient associated winds that transport moisture across the southern Indian Ocean and into East Africa (arrows in yellow boxes Fig. 5AB). Over the southern Indian Ocean (~60-110°E, between ~30°S and 5°S), we see mean atmospheric heating values change from strong cooling to strong heating. This atmospheric heating gradient is also associated with a strong meridional sea level pressure gradient that drives easterly moisture transports that drives easterly moisture transports that cross the equator and

feed moisture into EA. Longitude-by-height transects of climatological equatorial (5°S-5°N) ERA5 vertical velocities and zonal velocities reveal, on average, descending air tendencies between 40 and 55°E that heat and stabilize the atmosphere over the eastern Horn of Africa (Fig. 5C). Thus, we see in terms of the long-term mean climate over the Indian Ocean offsetting contributions from atmospheric heating over the Indian Ocean Warm Pool. Over the southeastern Indian Ocean, the meridional gradient between extra-tropical cooling and tropical heating helps produce a strong pressure gradient associated with low-level moisture transports into EA (Fig. 5B), but over the western and central equatorial Indian Ocean a zonal east-west heating gradient (Fig. 5B) helps set up an east-west response in vertical velocities (Fig. 5C) that helps suppress rainfall over the eastern Horn.

We next explore ERA5 SSTs and atmospheric heating anomalies following the 12 recent post-1997 OND La Niña events, which we also refer to as 'MAM WVG events' (Fig. 5D-E), because all of these events have strong negative WVG values in MAM (Figure 2C). Composites based on actual MAM WVG values and EHoA MAM dry seasons all ressemble Fig. 5D-E. We chose to use OND La Niña events to emphasize opportunities for long-lead prediction of MAM droughts following La Niña-related OND dry seasons.

A composite mean of the post-OND-La Niña MAM SST anomalies has a WVG structure (Fig. 5D), but also reveals interesting SST cooling in the central Indian and warming in the southwestern Indian Ocean. This Indian Ocean SST gradient is associated with moisture transport anomalies that flow from over the southern Indian Ocean, and then turn east, towards the eastern Indian Ocean (Fig. 5E). These transport anomalies exhibit enhanced anticyclonic flow around that deflects moisture southward along the western flank of the Mascarene High. This is consistent with findings of Wainwright et al. [*Wainwright et al.*, 2019] indicating that the late onset in MAM rainfall is linked with warmer SSTs over the south western Indian Ocean by delaying the northward movement of the tropical rainfall belt.

These MAM WVG events are associated with large statistically significant changes in atmospheric heating in the Indo-Pacific Warm Pool (100-150°E,15°S-15°N) and Central Pacific (150°E-170°W, 8°S-6°N) (Fig. 5D, Table 2). These results identify a very large westward transition in equatorial western-central Pacific heating. Driven both by diabatic heating and heat convergence, these large shifts indicate a westward shift of peak atmospheric heating, with increased subsidence near the equatorial dateline, increased equatorial Pacific moisture and heat transports, and increased Warm Pool heating.

Over the Indian Ocean we also see an interesting, and statistically significant, increase in atmospheric heating over the Northern Indian Ocean (60-100°E, 15°S-6°N), and some small atmospheric heating decreases over the central Indian Ocean (60-100°E, 15°S-6°N) (Fig. 5E). Dry season SST composites (Fig. 2A) show fairly large (-1.2 to -0.6Z) and significant cooling anomalies over the central Indian Ocean as well, contributing to an enhanced equatorial SST gradient between the central Indian Ocean and the Warm Pool. Increased Warm Pool and North Indian Ocean atmospheric heating, combined with less heating over the Central Indian Ocean appears associated with anomalous westerly moisture transports across the equatorial Indian Ocean, away from EA. This can be seen as an eastward shift of the climatological transport fields, which typically flow into EA (Fig. 5B). These exchanges of heat and moisture modulate

the Walker Circulation, increasing heating and moisture convergence over the Warm Pool and northern Indian Ocean, and decreasing these quantities over the central Indian and Pacific Ocean. Table 2 lists the diabatic heating, heat convergence, and moisture convergence anomalies for recent WVG events and 1981-2022 dry EA MAM seasons. Energy terms are in Wm^{-2}, while moisture convergence is in total mm per MAM season. Increases in convergence in the Warm Pool and Northern Indian Ocean are highly significant and large.

As discussed in the methods section, areas of increased or decreased atmospheric heating also correspond to areas with decreasing or increasing divergence of geopotential height energy (Fig. 4), because heating and geopotential height energy are tightly coupled in a hydrostatic atmosphere [*Peixoto and Oort*, 1992]. In the Central Pacific and Central Indian Ocean, increased geopotential height energy stabilizes the atmosphere and increases surface pressures. Conversely, in the Warm Pool and northern Indian Ocean, we find increased height divergence and lower surface pressures. This supports strong zonal moisture and heat transport anomalies flowing from over the Central Indian and Pacific into the Warm Pool (Fig. 5E).

Correlations of equatorial 1981-2022 WVG/ERA5 vertical and zonal velocities and specific humidity (Fig. 5F) reveal a Walker Circulation enhancement, consisting of a Warm Pool versus central Pacific dipole, and a weaker but still significant response over the Indian Ocean. The latter appears associated with subsidence in the middle and lower troposphere, westerly wind anomalies, and reduced atmospheric water vapor in the lower half of the troposphere between 40°E and 100°E. As discussed above, climatological conditions relate equatorial Indian Ocean Warm Pool atmospheric heating to offsetting factors: moisture transports across the southern Indian Ocean (Fig. 5AB), and subsidence between 40-55°E. WVG events increase atmospheric heating over the northern Indian Ocean and decrease atmospheric heating over the central Indian Ocean (Fig. 5E, Table 2), while also increasing the zonally overturning Walker Circulation (Fig. 5F). Over East Africa, this reduces atmospheric moisture and vertical motions in the mid-troposphere (Table 3).

Strong links between an enhanced Walker Circulation and dry outcomes during the EA MAM season are shown in Figure 6A,C. These scatterplots identify the very strong covariation between Warm Pool heating and moisture convergence (ERA5 R=0.99, MERRA2 R=0.98, p=0.0001). This strong correlation is not surprising. Heat and moisture transports are very similar, being driven primarily by low-level winds. Increased moisture convergence increases precipitation and latent heating (Eq. 4). More moisture increases the trapping of longwave radiation. What is striking, however, is 1) how variable these terms are, and 2) how well intense heating and moisture convergence discriminates dry EA seasons, as indicated by the circle colors.

The first point matters. If year-to-year variations in the Warm Pool were small, they would not be likely drivers of EA droughts. But what we see in the ERA5 and MERRA2 are very large ranges, with heating and moisture convergence ranging from ~150 to ~700 Wm^{-2} and ~50 to ~350 $mmMAM^{-1}$. These data exhibit a ~six-fold change between the weakest and strongest seasons. During the more intense seasons, when ERA5 heating exceeds ~500 Wm^{-2}, as indicated by the vertical black line in Fig. 5A,C, we see frequent dry EA outcomes and few wet or normal seasons. Furthermore, the circle with black crosses reveal that many of these strong heating/convergence years are strong MAM WVG events that followed OND La Niñas. OND La

Niñas are very robust indicators of strong MAM Warm Pool heating and moisture convergence … up to six months in the future. Interestingly, the 2018 WVG was associated with low heating and convergence values, and very heavy rains, likely due to the influence of sub-seasonal MJO and cyclone influences [*Kilavi et al.*, 2018]. It should be noted, also, that moderate and low heating/convergence outcomes have few droughts, but there does not appear to be a strong connection to wet season frequencies. These results support the idea that dry seasons are predictable because of links to Pacific SSTs (Fig. 2A), while wet seasons are less predictable (Fig. 2B), because forcing from Warm Pool is limited.

Scatterplots showing Warm Pool heating and Western V SSTs (Fig. 6B,D) also support links between Western V warming, Walker Circulation enhancements and frequent EA droughts. Warm Pool heating is strongly linked to warmer Western V SSTs. The 1981-2022 correlations between Western V SSTs and ERA5 and MERRA2 atmospheric heating are 0.74 and 0.70 (df. 40, p=0.0000001). Very warm Western V SSTs are clearly associated with increased Warm Pool atmospheric heating, and when Western V SSTs exceed +0.8Z, we find frequent dry EA rainy seasons (8 out of 12 seasons). We have already discussed the strong link between Western V SSTs and human-induced warming (Fig. 3A,B).

Past research [*Funk et al.*, 2018; *Funk et al.*, 2019] has described how warm Western V and Western North Pacific SSTs are associated with ridging aloft, producing high pressure anomalies that encircle the twin equatorial upper lows associated with La Nina events, as represented by the Matsuno-Gill model [*Gill*, 1980]. The twin upper-level lows are at ~150°W, at ~15°S and 15°N; while upper-level ridging is located both in the extra-tropical Pacific (~170-150°W, ~45°S and ~45°N) and over the equatorial Western Pacific (~150°E, 20°S-2-°N; Figures 5 and 6 in reference[*Funk et al.*, 2018]). These figures show that the resulting geopotential height gradients disrupt the sub-tropical westerly jets, increasing upper-level geopotential height convergence near the equatorial Central Pacific, amplifying the easterly flows of heat and moisture into the Warm Pool, and disrupting the Indian Ocean branch of the Walker Circulation.

Figures 5 and 6 highlight opportunities for prediction. As highlighted by the repeated use of green crosses, OND La Niñas are associated with predictable negative MAM WVG values (Fig. 2C) and strong Warm Pool atmospheric heating, and moisture convergence, and very warm Western V SSTs (Fig. 6). Over eastern East Africa, ERA5 and MERRA2 indicate highly significant and large (~-1 sigma) decreases in total precipitable water during strong WVG MAM seasons; in the mid-troposphere subsidence also increases significantly (Table 3). Often arising in conjunction or after an OND La Niña event, these teleconnections set the stage for sequential but often predictable dry seasons. Thus La Niña-related MAM droughts are predictable because of reliable and predictable WVG conditions (Fig. 2D, 5D), and Walker Circulation enhancements (Fig. 5E, Fig. 6).

This section has focused on the 1981-2022 satellite-observation period, for which we have good rainfall observations, reanalyses and SSTs. Over this period, we can say with great certainty that most MAM EA dry seasons were associated with more heating and moisture convergence in the Warm Pool and northern Indian Ocean, following La Niñas, when there have been predictable very warm Western V and WVG SST conditions. We next shift to a 1950-2022 time period to

examine the 'East African Enigma', to better understand some of the predominant features that differentiate "modern era" post-1997 La Niña events from earlier ones.

4.3 Contrasting MAM circulations following 1998-2022 and 1950-1997 OND La Niñas

An important, but analytically challenging, aspect of the EA Paradox is a potential shift in links to La Niña. There is general agreement on a shift in Pacific SST following the 1997/98 El Niño [*L'Heureux et al.*, 2013; *Lyon et al.*, 2013; *Yang et al.*, 2014]. Following this event, Western V SSTs increased [*Funk et al.*, 2019] and the Western V Gradient decreased substantially (Fig. 2C). Since the early 2010s, it has been hypothesized that the interaction of La Niña events and a low-frequency warming [*Williams and Funk*, 2011] may enhance the link between La Niña and dry EA MAM seasons, and recent work on this important topic [*Park et al.*, 2020] shows clearly the increasing correlation between boreal winter ENSO SSTs and EA rains in the following MAM season. Park et al. (2020) describe how a westward intensification of the Walker Circulation enhances links to Pacific SST variations, with 2000-2016 zonal equatorial vertical velocities, 200 hPa velocity potential and winds exhibiting ENSO teleconnections between 50°E and 180°E.

The recent availability of 1950-2022 ERA5 reanalysis, gives us an exciting opportunity to map the change in atmospheric heating and moisture convergence during the MAM seasons following the 12 post-1997 OND La Niñas versus the 12 1950-1997 La Niñas. While not identical, these results (Fig. 7A) broadly resemble WVG events (Fig. 5E), this implies a change in the behavior of the 'modern' MAM seasons that follow OND La Niñas. Fig. 7A indicates stronger atmospheric cooling and higher low-level air pressures over the southeastern Indian Ocean and central Indian Ocean, and an interesting negative IOD-like heating increase in atmospheric heating over the eastern equatorial Indian Ocean, i.e. an intensification of the Indian Ocean branch of the Walker Circulation. This increased atmospheric heating appears associated with higher pressures over the central Indian Ocean, and northward moisture transport anomalies that cross the equator near 75°E and turn towards Indonesia. In a sense, the eastward edge of the climatological moisture transports over the Indian Ocean (Fig. 5A) has shifted east, increasing over the central Indian Ocean (yellow arrow in Fig. 7A). Stronger eastward transports from over the central Pacific feed more heat and moisture into the Indian Ocean Warm Pool. This pattern is not associated with the western Indian Ocean, but rather the difference between the tropical central Indian Ocean and the Indo-Pacific Warm Pool, where WVG SST composites also indicate a dipole structure (Fig. 5D,E).

Given the strong relationship between dry EA seasons and Warm Pool atmospheric heating (Fig. 6A,C), we can contrast ERA5 MAM Warm Pool heating Probability Distribution Functions (PDF) for pre-and-post 1997 La Niña events (Fig. 7B). A ~110 Wm^{-2} increase in heating is identified, and this distribution shift increases the probability of exceeding a 500 Wm^{-2} threshold from 24% to 58%. Recent OND La Niñas anticipate much more energetic MAM Walker Circulations. These results can help explain why predicted WVG events (Fig. 2D) are good indicators of elevated EA MAM drought risk, and why there has been a large shift in EA MAM SPI PDFs following pre-and-post 1998 La Niña events (Fig. 7C). Since 1998, when there has been an OND La Niña, there have been strong MAM WVG gradients (Fig. 2C), very warm Western V SSTs (Fig. 5D), and strong Warm Pool heating and convergence (Fig. 6). These

results, and the large and significant changes shown in Fig. 7A, help explain why 75% of the time EA MAM rains are poor, when a La Niña arrives during boreal fall.

It is important to note, however, that dry EA MAM seasons are linked to the overall Pacific SST gradient structure, not just the NINO3.4 region (Fig. 2A). For example, during three of the nine seasons with boreal fall La Niña and dry MAM outcomes (2001, 2009, 2017), NINO3.4 SST values did not meet the ONI La Niña criteria during MAM, yet these seasons had strong negative WVG values and large Warm Pool heating values [>460 Wm^{-2}]. Looking to the large-scale WVG more extensively resolves the large-scale SST patterns that arise from the interaction of natural ENSO variability and anthropogenic warming trends. The next section discusses the latter more in detail.

4.4 Relating Warm Pool heating and more frequent droughts to anthropogenic warming in the Western V

We next explore low frequency (20-yr) links between MAM Pacific SSTs, Warm Pool heating, and EA dry season frequencies. The value of diagnostic analyses focused on atmospheric heating and moisture transport/convergence patterns (i.e. sections 4.2 and 4.3) is that they enable us to quantify the changes in climatic forcing associated with SST gradients. The WVG, by itself, is somewhat arbitrary, given that we weight equally the standardized Western V and NINO3.4 regions. While studies examining the ENSO-residual West Pacific Warming Mode (WPWM) have suggested that Western V-like SSTs amplify the Walker Circulation [*Funk and Hoell*, 2015; 2017], an important question that we address here is '*how influential is the Western V, in comparison with ENSO, as represented by NINO3.4 SST*?'.

To set the stage for this analysis, we briefly present an updated analysis (Fig. 8) of the 1900-2022 ENSO and WPWM principal components (PC), as in Funk and Hoell (2015). ENSO in this study, as in [*Lyon et al.*, 2013], is represented by the first EOF/PC of tropical Pacific SSTs. This PC tracks closely with SST in the NINO3.4 region (Fig. 8A). The ENSO PC and NINO3.4 average SST time-series have a 1950-2022 correlation of 0.94. To estimate the WPWM, each grid cell's MAM SST is regressed against the ENSO PC. Then the 1st EOF of the global residuals is used to define the WPWM, which tracks closely with the Western V. The WPWM PC and Western V average SST time-series have a 1950-2022 correlation of 0.87. An identical calculation of the WPWM, based on large ensembles of climate change models, are very similar to the observed patterns [*Funk and Hoell*, 2015; 2017]. Western V warming is not primarily driven Pacific Decadal Variability. Time-series of the WPWM/ENSO PCs (Fig. 8C) and Western V/NINO3.4 (Fig. 8D) are very similar. In broad strokes, two transitions appear in these time-series. First, the ENSO/NINO3.4 time-series have a Pacific Decadal Oscillation-related [*Mantua and Hare*, 2002] increase in the late 1970s, but thereafter show little increase [*Seager et al.*, 2022]. Then, the WPWM/Western V trends upward, with post-1998 values being especially warm. It is worth noting that the MAM 2022 WPWM and Western V values appear to be, by a substantial margin, the warmest on record.

We next use linear regression to relate 20-yr MAM Western V and NINO3.4 SST values to 20-yr 1950-2022 ERA5 Warm Pool atmospheric heating. The blue bars in Fig. 9A show 20-yr average ERA5 Warm Pool Atmospheric heating. Between the first and last 20-year period we see a

683 substantial increase, from ~330 to ~420 Wm^{-2}. Interestingly, a regression based on 20-yr
684 standardized Wetsern V and NINO3.4 SST can explain 97% of the atmospheric heating variance.
685 The Western V and NINO3.4 coefficients are highly significant and roughly similar in
686 magnitude (58 and 67 Wm^{-2} per standardized anomaly). These results are shown with a green
687 line in Fig. 9A. A regression carried out with just 20-yr Western V (red line Fig. 9A) explains
688 76% of the observed variance. Most of the 20-yr variance of the Warm Pool heating can be
689 explained by Western V warming. To examine the contribution of climate change, we can use
690 this equation ($HEAT_{WV}$ = 386 + 44*Western V SSt), but replace the observed Western V values
691 with the median of our large CMIP6 ensemble (Fig. 3A). These results are labeled as F(WestV-
692 CMIP6-50th Percentile SST) in Fig. 9A. 20th and 80th percentile CMIP6 estimates are also shown.
693
694 We would interpret these results as follows. First, the WVG formulation, which gives equal
695 weight to the Western V and NINO3.4 regions, seems fairly justified at 20-yr time-scales. 20-
696 year Warm Pool atmospheric heating covaries with both 20-yr NINO3.4 and Western V SSTs,
697 which in turn track closely with the first two models of global SST variability (Fig. 8). Between
698 the 1970s and 1990s a largely natural increase in NINO3.4 SSTs occurred [*Mantua and Hare*,
699 2002] (Fig. 3C), and we also see this reflected in the Warm Pool heating regression estimate,
700 which declined by about 40 Wm^{-2} during this period. However, since the 1980s, the Western V
701 warmed substantially, and we find this associated with a large ~80 Wm^{-2} increase Warm Pool
702 heating.
703
704 Is the recent Western V warming largely due to climate change, or natural decadal variability?
705 While some studies, using detrended SSTs, have argued that western Pacific warming is largely
706 natural [*Lyon*, 2014; *Yang et al.*, 2014], it is possible that the detrending process used in these
707 studies introduces biases into the results, since the rates of external forcing and associated
708 warming increase non-linearly. Assuming climate change is linear, and that residuals are
709 'natural' can miss the rapid human-induced warming present in the 1990s-2020s (Fig.3A). A
710 simpler approach is to compare directly observed 20-yr Western V SSTs with estimates from the
711 CMIP5 [*Funk et al.*, 2019] or CMIP6 (Fig. 3A, Fig. 8A). CMIP6 20-yr Western V SST tracks
712 extremely well with the observations (median time series, R=0.98, 1950-2022). The heavy black
713 line in Fig. 9A translates the median CMIP6 Western V SST values into Warm Pool atmospheric
714 heating, in Wm^{-2}, using the empirical Western V regression coefficients. Differences between the
715 observed (red line) and externally-forced CMIP6 (heavy black line) 20-year Western V time-
716 series indicate the influence of natural Pacific Decadal Variability. These fluctuations are limited
717 to a small cooling in the 1980s and warming in the late-2000s. The dominant change in observed
718 20-yr running average Western V (red line) - the increasing trend - aligns with human-induced
719 warming (black lines). Between 1950 and 2022, CMIP6 Western V SST estimates suggest an
720 overall increase in Warm Pool atmospheric heating from ~340 to ~410 Wm^{-2}. This shift in mean
721 Warm Pool heating is augmented further following recent La Niña events (Fig. 7A), helping to
722 explain the enigmatic increase in dry EA MAM seasons (33%→75%, Fig. 7C).
723
724 Over the past 75 years, Western V SST have warmed by ~+2Z standardized anomalies, and this
725 warming shifts the heating distribution by more than +80Wm^{-2}. Projections through 2050 suggest
726 another similar increase over the next 30 years (Fig. 9A). Such heating influence will likely be
727 particularly dangerous during or following La Niñas, setting the stage for more frequent
728 sequential OND/MAM drougths.

In contrast to Western V SSTs, there is a large and growing discrepancy between observed east Pacific SSTs and CMIP6 projections, with "*observations-based SST trends … at the far edge or beyond the range of modeled internal variability*" [*Seager et al.*, 2022], there has been a notable lack of warming in the NINO3.4 region, and this is in marked contrast to 20-yr anomalies from a 25-model 152-member ensemble of CMIP6 simulations (Fig. 3D). The observed 2003-2022 value (-0.09Z) is extremely unlikely given the distribution from the CMIP6 simulations (Supplemental Fig. 4B). More detailed analyses [*Wills et al.*, 2022] identify "*a triangular region in the eastern tropical and subtropical Pacific*" as the ocean region where CMIP6 model simulations differ most from observations, with the differences very unlikely (<5% probability) due to internal variability. While a detailed exploration is beyond the scope of this study, systematic Pacific SST biases are one likely cause of this discrepancy, and when bias-corrected ocean and atmosphere models are used to explore this issue, they recreate the observed increase in equatorial Pacific zonal SST gradients [*Seager et al.*, 2019]. Hence assuming that the climate change models are 'correct' and that the observed lack of warming is driven by naturally-occurring Pacific Decadal Variability appears problematic.

Finally, we present regressions relating 20-yr NINO3.4 and Western V SSTs to 20-yr dry season frequencies, i.e. the number of times in each 20-yr period in which EA MAM SPI was less than -0.44Z (Fig. 9B). The F(Observed WestV SST) time-series denotes a set of probability estimates derived via a linear regression using observed Western V SSTs as a predictor and 20-yr running observed frequencies of dry East African seasons as a predictand: ($PROB_{dry} = 0.3+0.13WV$, $R^2=0.74$). Western V SST increases can explain most of the 20-yr variance in 20-yr changes in the frequency of dry seasons. These results suggest that the Western V warming has been a primary driver of increased dry season frequencies in the eastern Horn of Africa. Since Western V warming has been dominated by human-induced external forcing, climate change has been a strong driver of increased dry season frequencies in East Africa.

5 Conclusions

5.1 A Walker Circulation intensification can explain the enigma predictability of the EA MAM rains.

Here, we have addressed a quite specific question – do intensifications of the Walker Circulations help explain the "East Africa Climate Enigma', i.e. the fact that so many recent OND La Niñas are followed by below-normal MAM EA rainy seasons. Furthermore, how does this link relate to climate change and the large observed decline in EA MAM rains (Fig. 1B)? We have addressed these questions in a two-step attribution process. The first step links observed EA droughts to decreasing but predictable WVG values (Fig. 2). These strong Pacific gradients, we argue, are being produced through an interaction of naturally occuring La Niña events and human-induced warming in the Western V region (Fig. 2C, Fig. 3A,B). The second step then links WVG events to changes in the Walker Circulation and conditions over EA (Fig. 5-6, Tables 2,3).

These 1981-2022 results paint a clear story that helps us understand the predictability of MAM dry seasons. First, we see a large, climate-change-related warming of the Western V region, well-reproduced in the CMIP6 (Fig. 3A,B). This warming, combined with the influence of La Niña, results in very reliable low WVG values during MAM seasons following OND La Niñas (Fig. 2C). These gradients, furthermore, are predicted well by seasonal climate prediction systems (Fig. 2D). MAM EA rains, furthermore, have very often been poor following post-1997 OND La Niñas (Fig. 7C), consistent with increasing ENSO teleconnections [*Park et al.*, 2020].

To make such insights more actionable, however, we have tried to provide a clear causal description linking WVG conditions to dry EA rains. To this end we have used gradients in atmospheric heating to help describe the Indo-Pacific Walker Circulation. In terms of the long term mean climate, these fields identify the regions of high and low pressure that help guide moisture transports into the Warm Pool and eastern Horn (Fig. 5B), which in turn help setup zonally-overturning wind patterns along the equator (Fig. 5C).

Composites of SSTs, atmospheric heating and moisture transports, following post-1997 La Niñas, show significant and substantial changes changes in SSTs (Fig. 5D) and atmospheric heating and moisture transports (Table 2, Fig. 5E). These large and significant changes (Table 2) can be anticipated many months ahead of the MAM rains, since these composites are based on lagged OND La Niña definitions. Warm Pool intensification arises through both increased diabatic heating and increased heat and moisture convergence (Table 2). Over EA, we find corresponding decreases in total precipitable water and increases in mid-tropospheric subsidence (Table 3).

Scatterplots of Warm Pool atmospheric heating and moisture convergence (Fig. 6A,C) very strongly support the link between Walker Circulation enhancements and dry EA outcomes. When ERA5 heating exceeded 450 Wm^{-2} there were 9 dry seasons, 2 normal seasons and 2 wet seasons. Strong Warm Pool heating in MERRA2 reanalyses similarly discriminate dry outcomes. As previously hypothesized, Walker Circulation enhancements are a robust indicator of dry EA outcomes. Twelve post-1997 La Niñas were precursors to MAM SST anomalies (Fig. 5D) that strongly resemble dry season SST composites (Fig. 2A). And the associated circulation disruptions (Fig. 5E, Fig. 7AB, Table 2) appear linked to frequent droughts (Fig. 1B), but offer opportunities for prediction (Fig. 2D). The energetic framework provided here helps us explain these opportunities. While we only have ~12 events, we see that Warm Pool heating and moisture convergence increases dramatically during most of these seasons (Fig. 6A,C) and when compared to the MAM seasons following 1950-1997 La Niñas (Fig. 7A-B).

Thus, without ruling out other influences such as westerly Congo Basin moisture transports and the MJO [*Finney et al.*, 2020], or sub-seasonal changes in the length of the long rains [*Wainwright et al.*, 2019], the results presented here support the idea that one primary cause of recent EA droughts has involved a large westward shift in atmospheric heating between the equatorial central Pacific and Warm Pool regions during WVG seasons. These regions exhibit the largest atmospheric heating anomalies. But, as shown by Gill [*Gill*, 1980], increased heating in the Warm Pool may increase subsidence and low-level pressures to the west, changing circulation patterns over the Indian Ocean, providing proximate impacts that reduce moisture and vertical ascent over East Africa. Early studies linking EA drying with an increased Indian Ocean

branch of the Walker Circulation posited atmospheric heating over the central Indian Ocean [*Funk et al.*, 2008; *Verdin et al.*, 2005]; the work presented here suggests heating increases over Indian and Pacific Warm Pool regions, and underscores the amplifying role played by moisture and heat transports and convergence. This helps explains the link with Pacific SSTs [*Lyon and DeWitt*, 2012; *Yang et al.*, 2014] as well as the tendency for the long rains to start later and end earlier [*Wainwright et al.*, 2019]. Such insights could assist in the prediction of onset and cessation dates, which are linked to zonal wind variations over the Indian Ocean [*MacLeod*, 2018].

Our WVG composites (Fig. 5D) also identify Indian Ocean SST warming over the southwest and northern Indian Ocean, and cooling near 75°E,15°S. Recent analysis has suggested a later start and earlier cessation of the long rains [*Wainwright et al.*, 2019], and this may be consistent with the observed WVG SST responses, and expectations that La Niña-like conditions will tend to slow the onset and hasten then end of the rainy season. In the southern Indian Ocean, during WVG events (Fig. 5D), warmer southwestern SSTs could delay the typical northward progression of the rains between February and March. In the central and northern Indian Ocean, during WVG events (Fig. 5D,E, Table 2), warmer SSTs in the northern Indian Ocean (Fig. 5D) and increased atmospheric heating over the northern Indian Ocean, combined with cooler SSTs and less heating over the central Indian Ocean, might also help trigger an early transition to the boreal summer Indian Monsoon circulation, which could reduce rainfall in May. The contrasting heating responses over the northern and central Indian Ocean (Fig. 5E) help drive moisture and heat into the Warm Pool, and away from EA. This may suggest a 'Walker Circulation Intensification' over the northern Indian Ocean, perhaps leading to an earlier transition to a boreal summer monsoon pattern, similar to the June-August circulation. Hence, the increased frequency of strong WVG events, especially following recent La Niñas, appears related to the shorter EEA rainy season as described by Wainright et al. [*Wainwright et al.*, 2019]. Climate change assessments, based on regional climate model results [*Gudoshava et al.*, 2020], have suggested that the long rains will start and end earlier. This earlier start projection, which appears at odds with the observations, may be related to a tendency for the global climate change models to predict an El Niño-like tendency in Pacific SSTs (Fig. 3C,D), and the well-established north-south rainfall dipole associated with ENSO, with southern (eastern) Africa being drier (wetter) during El Niños.

In our La Niña atmospheric heating analysis (Fig. 7A), on the other hand, we find enhanced atmospheric heating primarily in the south-eastern Indian Ocean, where recent La Niñas appear associated with >160 Wm^{-2} more heating than pre-1998 events. In the absence of strong Walker Circulation forcing, sub-seasonal influences such as the MJO, and more local weather influences such as westerly Congo basin moisture transports likely play an important role [*Finney et al.*, 2020]. The MJO, of course, modulates the Walker Circulation and East African rains as well, and certainly influences heating and moisture transports. Recent research has linked a two-fold expansion of Warm Pool to a modulation of the MJO life cycle [*Roxy et al.*, 2019], with Maritime Continent residence times increasing by 5-6 days and Indian Ocean residence times decreasing by 3–4 days. Analyses of global satellite-gauge precipitation trends [*Adler et al.*, 2017], have noted marked increases WVG-like SSTs, Warm Pool total precipitable water and precipitation (c.f. their Fig. 8), consistent with a strong equatorial Pacific SST gradient [*Seager et al.*, 2022; *Seager et al.*, 2019].

In closing, when one considers the 'cause' of the EA rainfall decline, we would suggest that it is useful to consider two aspects: the increased impacts following recent La Niña events, and the high frequency of recent La Niña events themselves. In place of the 'East African Climate Paradox' we have suggested the 'East Africa Enigma': why have La Niña-related SST conditions become such a consistent driver of droughts during MAM? Our analysis of atmospheric heating and changes in moisture transports help explain how the combination of anthropogenic Western V warming and La Niña events leads to increases in Warm Pool heating, which in turn modulates important circulation features over the Indian Ocean, increasing subsidence and decreasing EA moisture levels (Table 3). Hence, the interaction of climate change and frequent La Niña events have led to frequent MAM droughts, and many of those dry seasons have followed poor OND outcomes [*Funk et al.*, 2018]. This is consistent with recent multi-agency alerts attributing the recent droughts to the combined influence of La Niña and climate change. Without climate change, there would not be a strong link to La Niñas (Figure 7A,B). It is worth noting that strong 'gradient La Niñas' have been identified in observations[*Johnson*, 2013], and are expected by climate change models [*Cai et al.*, 2022; *Cai et al.*, 2015a; *Cai et al.*, 2015b].

For EA, our study has emphasized the strong relationship between MAM atmospheric heating, WVG SST and EA SPI, given the set of all post-1997 OND La Niña events. Such conditions pose risks, even if a La Niña event fades. When these events commence, enhanced trade winds transport more oceanic heat energy from the east Pacific and into the Western V region, via the sub-tropical gyre, and there is a great deal of certainty that these transports will persist for many months. As oceanic heat content increases due to climate change, it is not surprising to see that these natural La Niña transport patterns result in large increases in Western V SSTs, and more negative WVG values (Fig. 2C), which are very predictable (Figure 2D). Western V SSTs, even in the absence of very cool NINO3.4 SSTs, still increase flows of heat and moisture into the Warm Pool atmosphere, which increase the risk of dry EA rainy seasons. Even if the frequency of La Niñas were to decrease in the future, La Niñas will develop in an environment that is very warm- and likely even warmer than present-day- and the conditions in the Warm Pool and Western V will likely amplify the impacts of these La Niñas, setting the stage for sequential dry East Africa outcomes in OND and MAM. It is also possible, however, that observed streak of La Niñas will continue, due to a stronger zonal Pacific gradient. CMIP6-based projections of Warm Pool atmospheric heating, based on Western V warming, suggest a further ~80 Wm^{-2} increase by 2050 (Fig. 9A). Understanding the emergent links between La Niñas, WVG and the Walker Circulation will help anticipate and manage risks.

Acknowledgments

This research was supported by the United States Agency for International Development (USAID) (Cooperative Agreement #72DFFP19CA00001), National Aeronautics and Space Administration (NASA) GPM mission Grant 80NSSC19K0686, and the Bill and Melinda Gates Foundation contract INV-017546.

Availability Statement

905 Please also note that we have produced a Dryad Data Repository with the time-series analyzed in
906 this study. We have chosen a spreadsheet format to maximize accessibility. Even non-
907 programmers can verify the basic results from our study. It is available at the link below.

908 https://datadryad.org/stash/share/I2kn11CShPWoYDlUAA-La9IjaMHDmKLHoJzZYWCMmc8

909

910 **Tables**

911

912 **Table 1.** The CMIP6 SSP245 models and simulations used in this study.

Model Names	Number of Simulations
ACCESS-CM2	3
ACCESS-ESM1-5	11
CanESM5-CanOE	3
CanESM5	25
CMCC-ESM2	1
CNRM-CM6-1-HR	1
CNRM-CM6-1	6
CNRM-ESM2-1	9
EC-Earth3-CC	1
EC-Earth3-Veg-LR	3
EC-Earth3-Veg	5
FGOALS-g3	4
FIO-ESM-2-0	3
GFDL-ESM4	3
GISS-E2-1-G	10
HadGEM3-GC31-LL	1
INM-CM4-8	1
INM-CM5-0	1
IPSL-CM6A-LR	11
MIROC6	3
MIROC-ES2L	30
MPI-ESM1-2-HR	2
MPI-ESM1-2-LR	9
MRI-ESM2-0	1
UKESM1-0-LL	5
Total Number of Sims	**152**

913

914

915

916

Table 2. Dry-Versus-West EA seasons and strong WVG season anomalies for selected forcing regions. *,**,*** denote significance at p=0.1, 0.05, and 0.01, based on two-tailed T-tests. Moisture convergence is shown as the seasonal total moisture convergence.

	Warm Pool	Eq Central Pacific	Northern Indian	Central Indian
Dry Seasons				
Heat Convergence [Wm^{-2}]				
ERA5	$+78^{***}$	-85^{*}	$+51^{**}$	-32^{**}
MERRA2	$+95^{***}$	-130^{**}	$+42^{**}$	-14
Diabatic Heating [Wm^{-2}]				
ERA5	$+44^{***}$	-32	$+29^{**}$	-13^{**}
MERRA2	$+77^{***}$	-55^{**}	$+45^{**}$	+3
Geopotential Divergence [Wm^{-2}]				
ERA5	$+108^{***}$	-112^{**}	$+67^{**}$	-51^{**}
MERRA2	$+128^{***}$	-178^{**}	$+63^{**}$	-16
Moisture Convergence [mm]				
MERRA2	$+85^{***}$	-80	-45^{**}	-49^{***}
ERA5	$+102^{***}$	-128^{**}	-51^{**}	-27^{*}
Strong WVG Seasons				
Heat Convergence [Wm^{-2}]				
ERA5	$+123^{***}$	-178^{***}	$+81^{***}$	-49^{***}
MERRA2	$+133^{***}$	-206^{***}	$+74^{**}$	-36^{**}
Diabatic Heating [Wm^{-2}]				
ERA5	$+66^{***}$	-81^{***}	$+48^{***}$	-19^{**}
MERRA2	$+95^{***}$	-114^{***}	$+86^{***}$	-40
Geopotential Divergence [Wm^{-2}]				
ERA5	$+169^{***}$	-250^{***}	$+110^{***}$	-76^{***}
MERRA2	$+172^{***}$	-287^{***}	$+160^{***}$	-91^{**}
Moisture Convergence [mm]				
ERA5	$+121^{***}$	-206^{***}	$+77^{***}$	-75^{***}
MERRA2	$+126^{***}$	-243^{***}	$+81^{***}$	-59

Table 3. Strong WVG season anomalies for Eastern East African MERRA2 and ERA5 Total Precipitable Water and 600 hPa vertical velocities. *,**,*** denote significance at p=0.1, 0.05, and 0.01, based on two-tailed T-tests. Moisture convergence is shown as the seasonal total moisture convergence. Anomalies also expressed as standardized anomalies. Eastern East Africa region corresponds to 38-52°E, 5°S-8°N.

	Total Precipitable Water [kgm^2s^{-1}]	Total Precipitable Water [Z-score]	600 hPa vertical velocity [Pas^{-1}]	600 hPa vertical velocity [Z Score]
ERA5	-2.4***	-1.1Z***	+0.004**	+0.7Z
MERRA2	-2.2***	-1.0Z***	+0.003*	+0.5Z

Figures

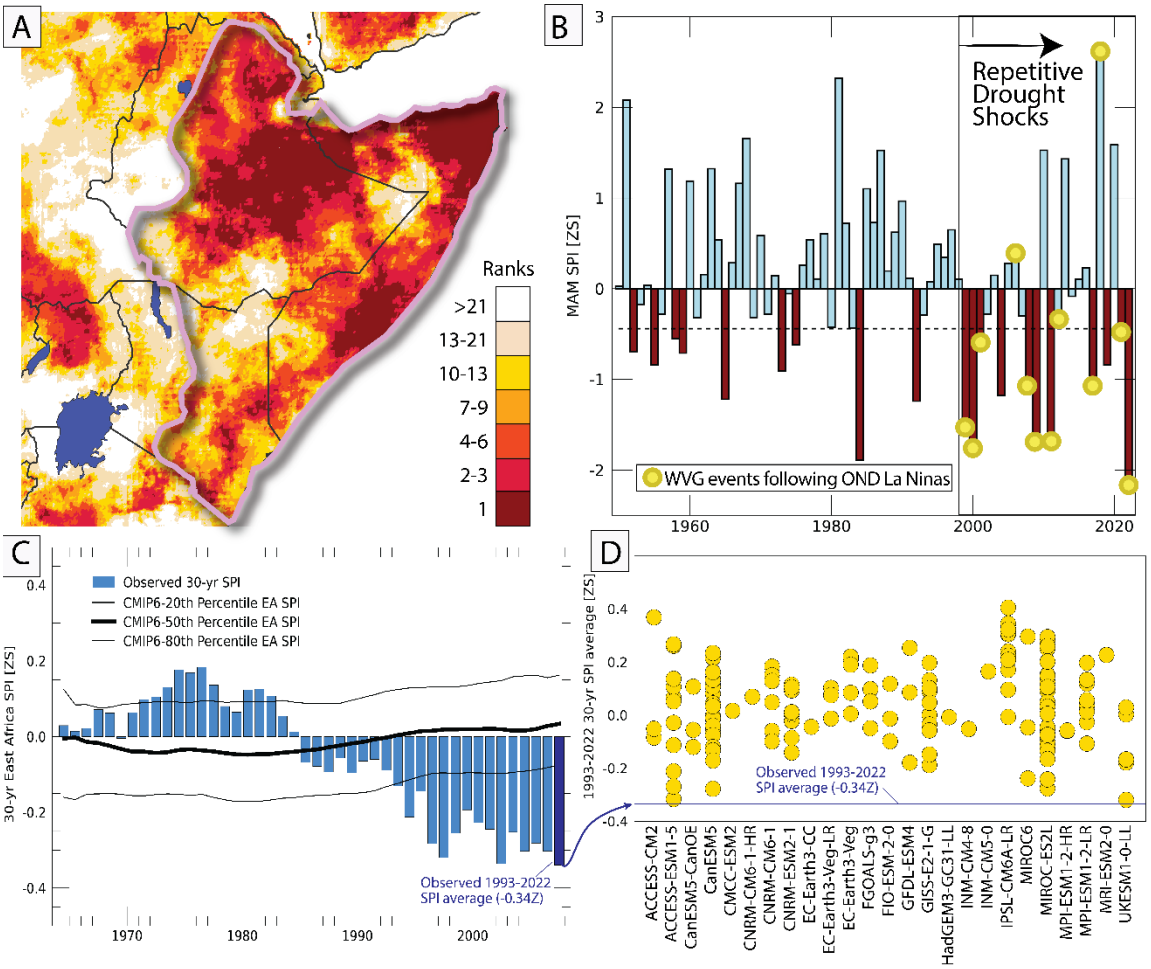

Figure 1. Describing the East African Climate Paradox. **A**. MAM 2022 rainfall ranks indicate most of the Horn of Africa received extremely low rainfall amounts, based on 42 years of CHIRPS rainfall. The purple polygon in Panel A denotes the area of exceptional dryness in MAM 2022. **B**. Time-series of dry region MAM CHIRPS/Centennial Trends rainfall, expressed as Standardized Precipitation Index (SPI) values). Also noted with yellow circles are strong negative WVG seasons. **C**. Observed (blue bars) and projected CMIP6 SSP245 30-yr average East Africa SPI. Centered on a 1981-2021 baseline. Based on 152 CMIP6 simulations. The thick and thin black lines show the median and 20th/80th quantiles of the CMIP6 simulation distribution. **D**. The 152 simulated CMIP6 2003-2022 20-yr average East Africa SPI, centered on a 1981-2021 baseline. The horizontal line in Fig. 1D denotes the observed 1993-2022 average East Africa SPI value (-0.34Z).

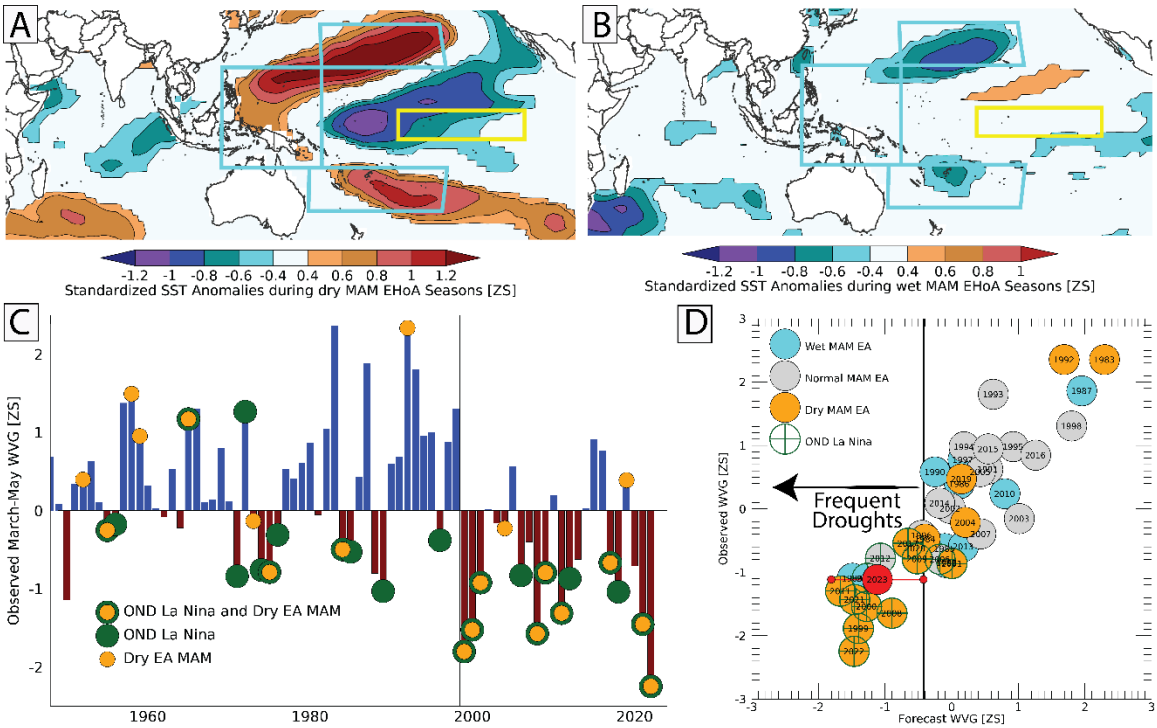

Figure 2. Relating dry seasons to the Western V gradient. **A-B.** Composites of standardized SSTs during 1981-2022 dry seasons (**A**) and wet seasons (**B**) reveal a substantial non-linearity. Dry seasons exhibit a coherent dipole pattern in the Pacific, while wet seasons SST anomalies exhibit few areas with significant relationships. Wet and dry seasons based on 1981-2022 EA SPI values of greater or less than +0.44 and -0.44. These breaks correspond with the top and bottom tercile boundaries. Screened for significance at p=0.1 using a two-tailed T-test. The cyan boxes in A and B denote the equatorial [120-160°E, 15°S-20°N], northern [160°E -150°W, 20-35°N], and southern [155°E -150°W, 30-15°S] regions of the 'Western V' area. The yellow box denotes the NINO3.4 region in the eastern equatorial Pacific [170-120°W, 5°S-5°N]. The WVG is the standardized difference between the NINO3.4 and Western V areas. **C**. A bar plot of observed standardized MAM WVG values, centered on a 1981-2021 baseline. Orange circles denote dry EA MAM seasons. Green circles denote preceding OND La Niña years. Orange within green circles identify OND La Niña seasons followed by dry EA MAM events. The thin vertical line at between 1998 and 1999 identifies the shift towards stronger WVG values and more frequent dry EA MAM rainy seasons. **D**. Scatterplot showing forecasts of MAM WVG index values, based on August NMME SST predictions. Observed MAM EA rainy season outcomes shown with blue/gray/orange shading. All time-series and SST centered on a 198)1-2021 baseline. Also shown are preceding OND La Niña seasons, and the 2023 WVG forecasts. The y-axis value has been set to the forecast value. 80% confidence intervals for the forecast are also shown with small red circles and a horizontal red line.

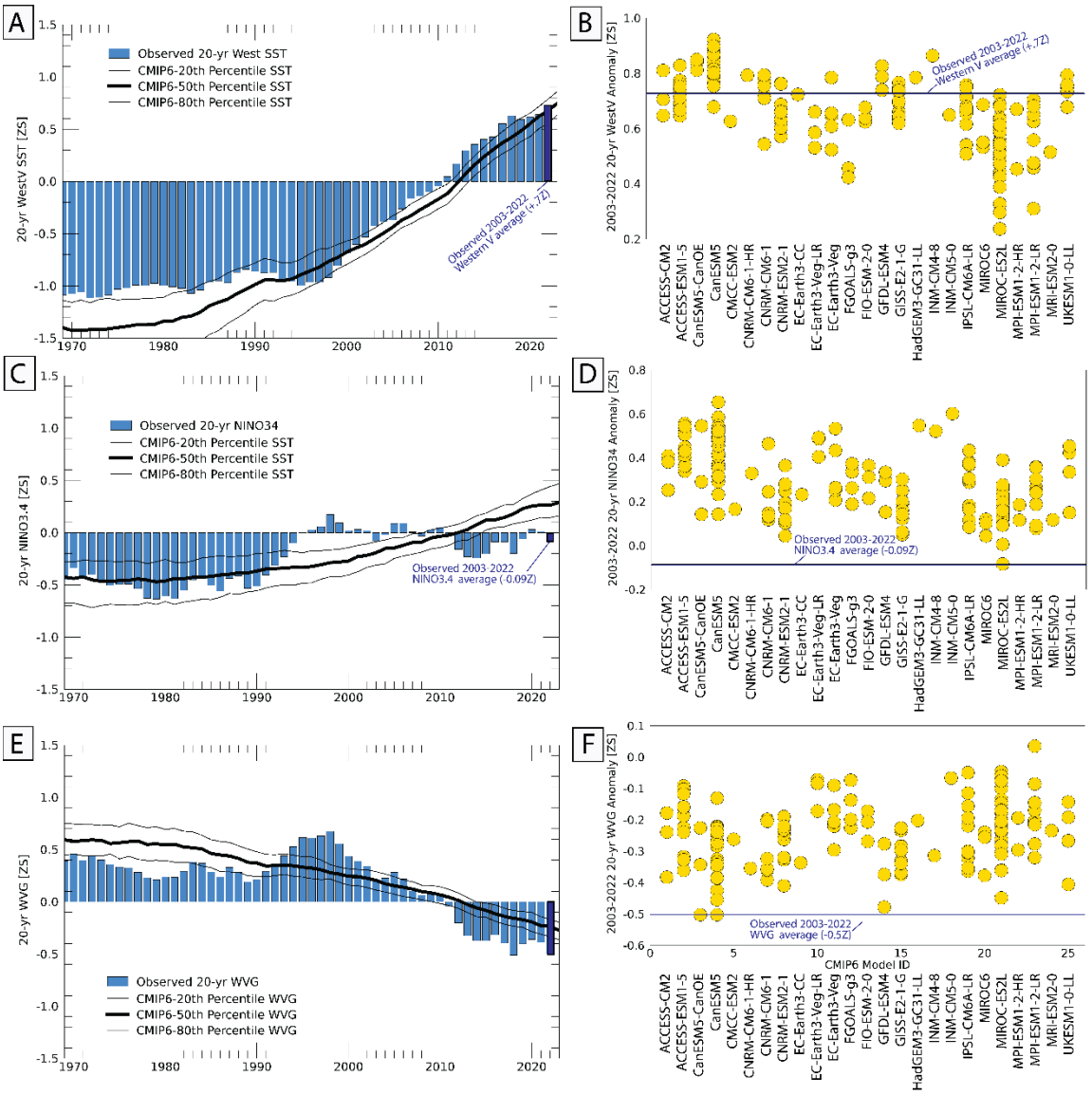

Figure 3. Observed and CMIP6 SST time-series. **A**. Observed (blue bars) and CMIP6 SSP245 projections of 20-yr averages of standardized Western V SST anomalies. Centered on a 1981-2021 baseline. CMIP6 results based on 152 CMIP6 simulations. The thick and thin red lines show the median and 20th/80th quantiles of the CMIP6 simulation distribution. **B**. Individual CMIP6 simulated 2003-2022 20-yr average Western V SST anomalies, centered on a 1981-2021 baseline. The horizontal line in Fig. 4B denotes the observed average 2003-2022 standardized Western V SST anomaly (+0.7Z). **C-D**. Same but for standardized NINO3.4 SST anomalies. **E-F**. Same but for standardized WVG index values.

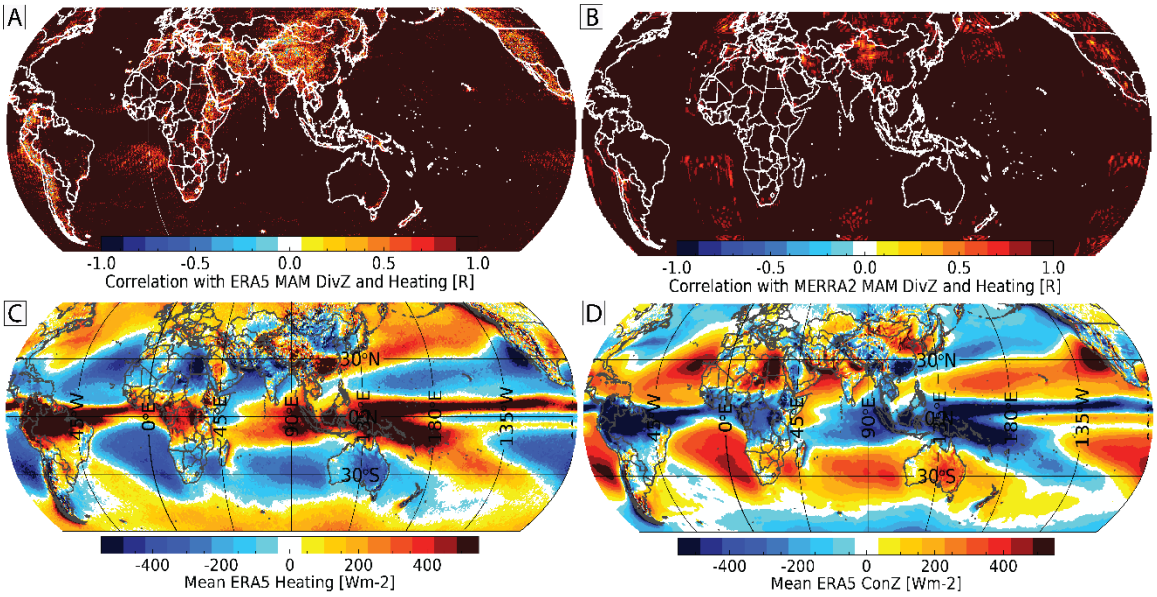

Figure 4. Geopotential height energy divergence offsets heating energy changes. **A-B.** 1981-2021 correlations between ERA5 (**A**) and MERRA2 (**B**) MAM atmospheric heating (diabatic heating + heat convergence) and geopotential height energy divergence. **C**. Long term (1981-2021) mean ERA5 atmospheric heating **B**. Same for geopotential height convergence.

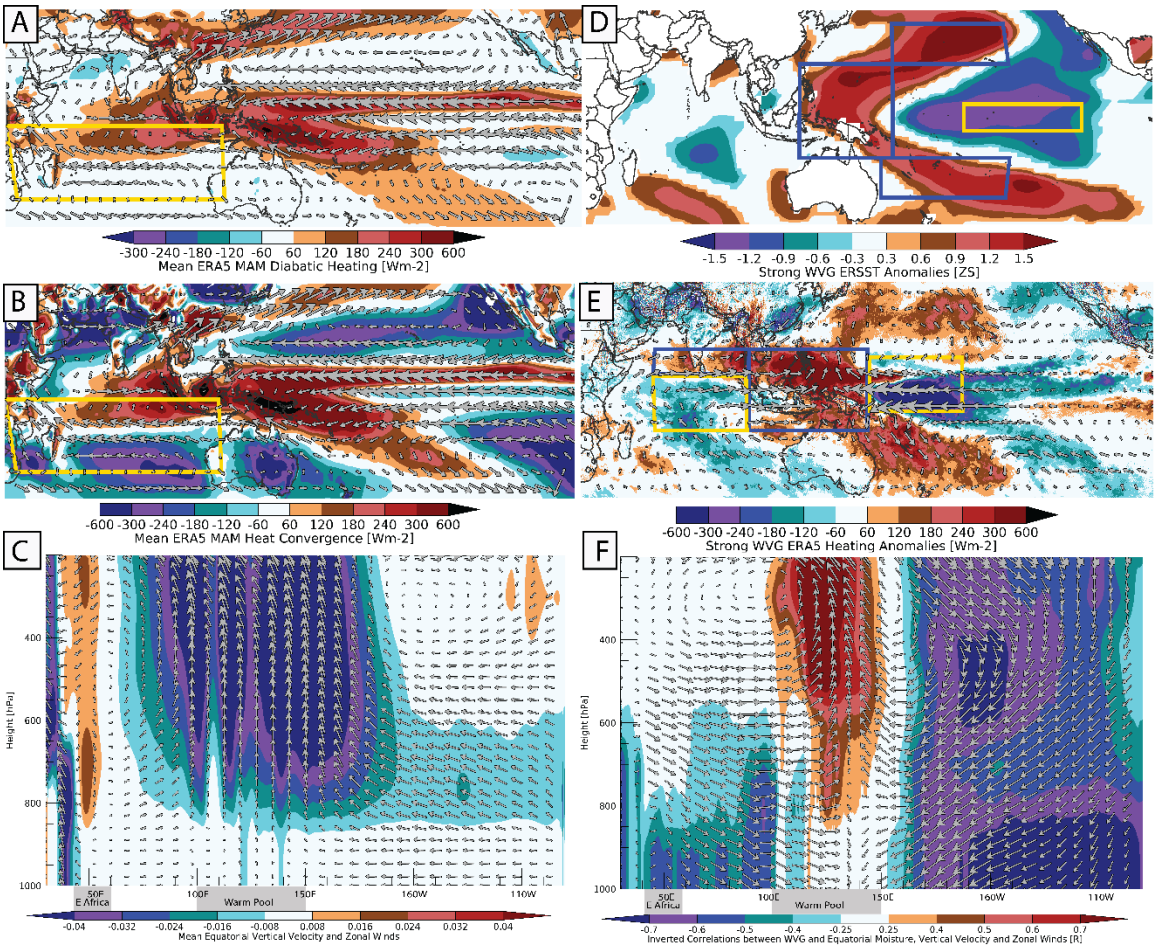

Figure 5. Relating WVG events to Walker Circulation intensification. **A**. Mean 1981-2021 ERA5 diabatic heating in Wm^{-2}. Vectors show ERA5 mean vertically-integrated moisture transports, with a maximum westerly flux rate of -357 $kgm^{-1}s^{-1}$. **B**. Same but for mean vertically integrated atmospheric heat convergence. **C**. Long term mean ERA5 equatorial [5°S-5°N] longitude-by-height vertical and zonal velocities (Pas^{-1} and ms^{-1}). Vertical velocities scaled by 200. **D**. Composites of standardized MAM SSTs during 1981-2022 strong WVG events (circles in Fig. 1B). Screened for significance at p=0.1 using a two-tailed T-test. **E**. Similar composites but for ERA5 atmospheric heating (diabatic heating + atmospheric heat convergence) in Wm^{-2}. Screened for significance at p=0.1. Also shown are ERA moisture transport anomalies, with a maximum westerly flux rate of -174 $kgm^{-1}s^{-1}$. Also shown are areas of interest: Indo-Pacific [100-150°E, 15°S-15°N], Central Pacific [150-170°E, 8°S-12°N], northern Indian Ocean [60-100°E, 5°N-15°N], and central Indian Ocean [60-100°E, 15°S-5°N]. **F**. 1981-2022 correlations between equatorial ERA5 vertical and zonal velocity and moisture (specific humidity) and inverted observed WVG values (the time-series shown in Supplemental Fig. 1A). Since negative vertical velocities (in Pas^{-1}) indicate upward motions (panel C), the vertical velocity correlations have been inverted, to indicate that stronger WVG values are associated with increased ascent over the Warm Pool.

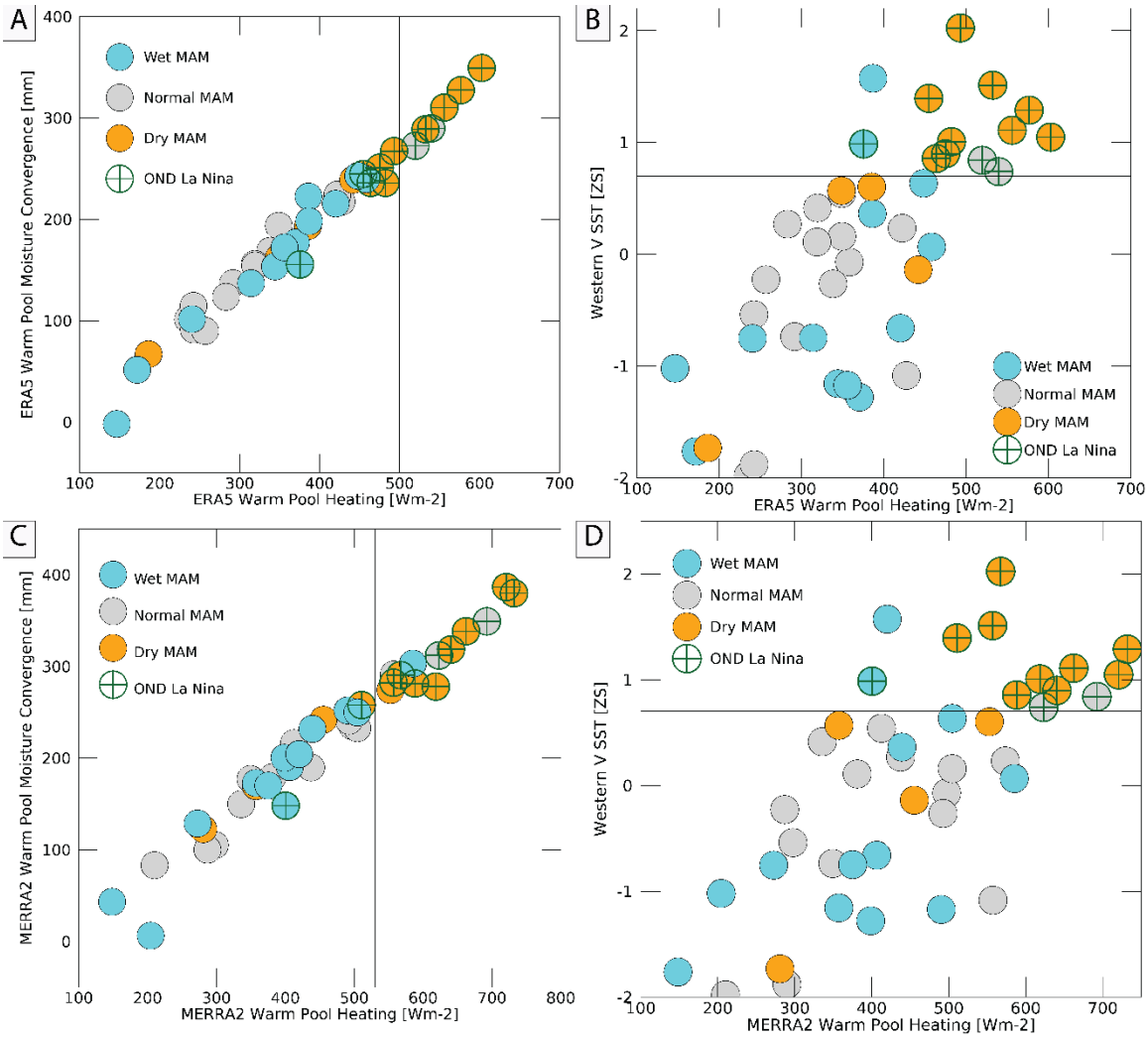

Figure 6. Increased Warm Pool atmospheric heating can help explain the East Africa Climate Enigma. Circle color denotes East African MAM rainfall terciles. Green crosses identify preceding OND La Niña seasons. **A**. A scatterplot of ERA5 MAM Warm Pool heating (x-axis) and Warm Pool moisture convergence (y-axis) **B**. A scatterplot of ERA5 Warm Pool heating (x-axis) and standardized MAM Western V SSTs (y-axis). Circle colors in **A** and **B** identify EA wet and dry MAM rainy seasons. **C-D**. Same but for MERRA2 reanalysis.

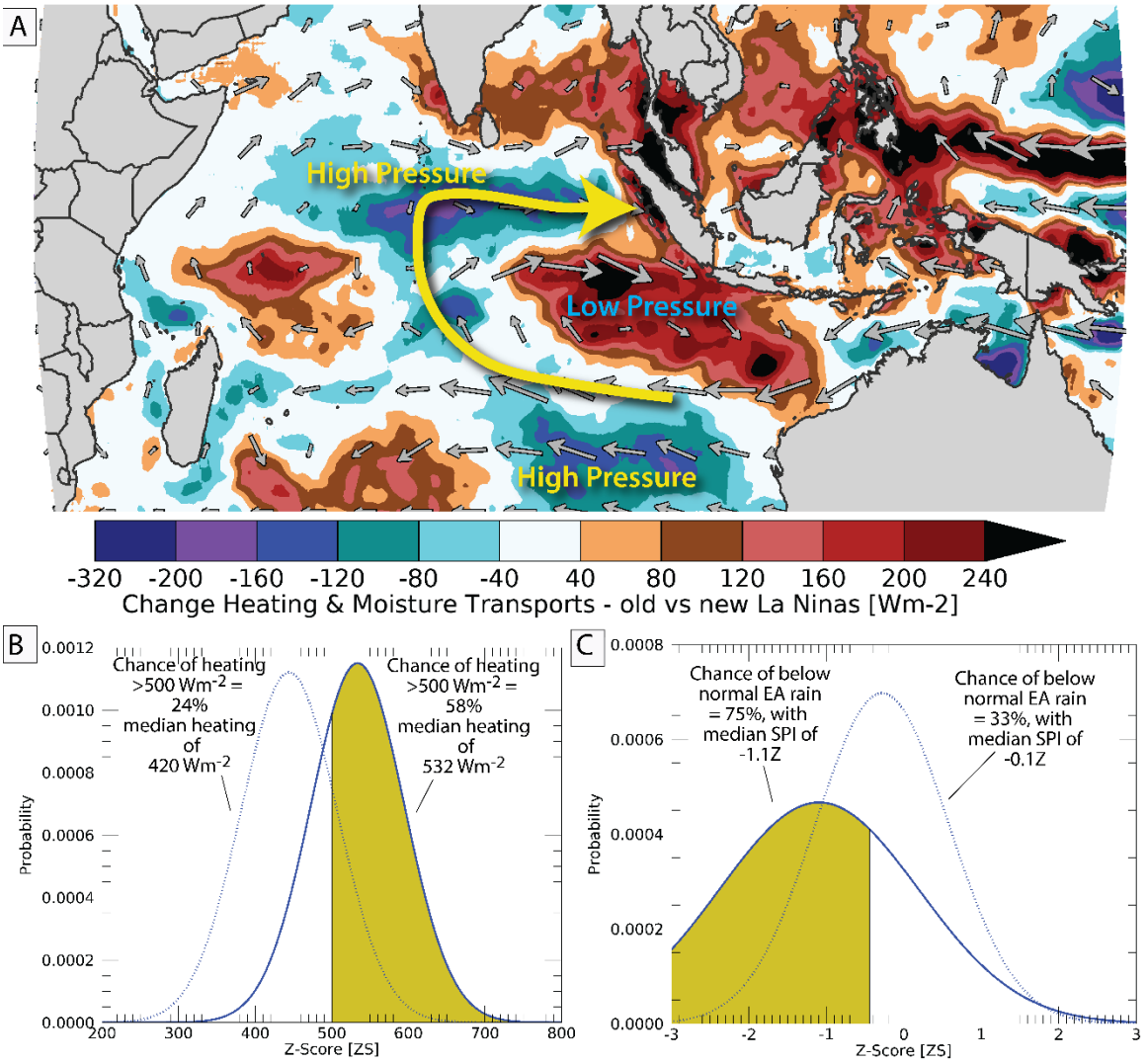

Figure 7. Change in atmospheric heating following recent La Niñas can help explain the East Africa Climate Enigma. Circle color denotes East African MAM rainfall terciles. Green crosses identify preceding OND La Niña seasons. **A**. The difference between 1999-2022 and 1950-1997 ERA5 atmospheric heating and moisture transports in MAM seasons following OND La Niña events. **B**. PDFs of MAM West Pacific heating following pre- and post-1998 OND La Niña events. **C**. Same for observed EA MAM SPI (i.e. the data plotted in Figure 1B).

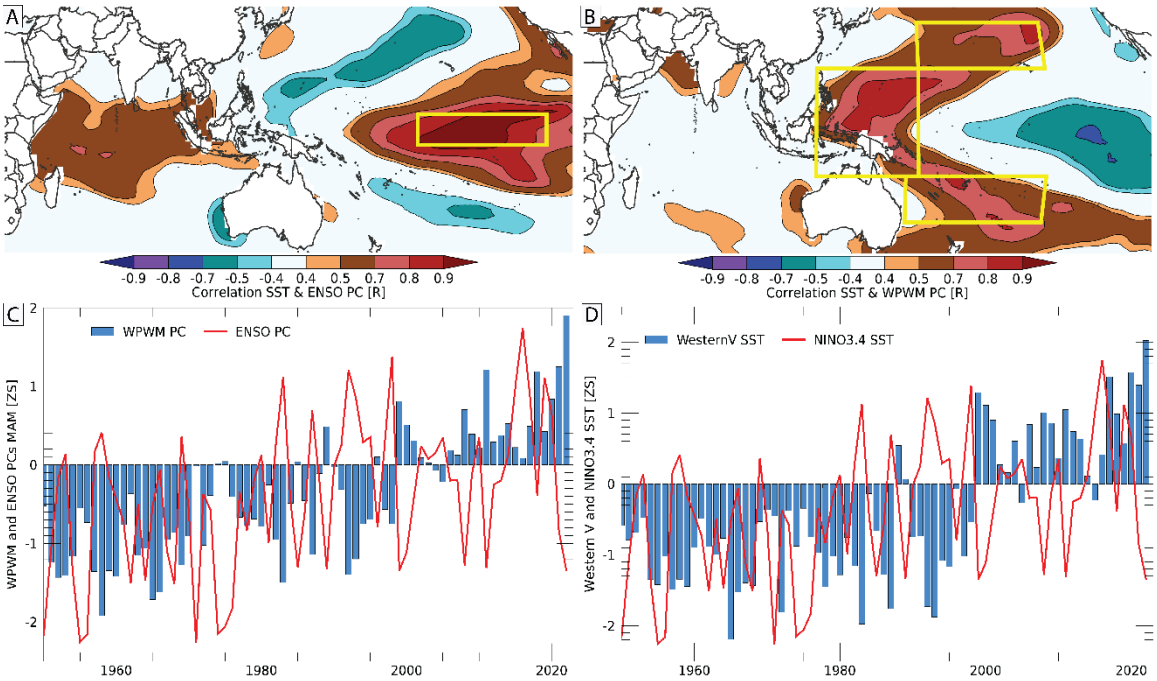

Figure 8. Relating MAM NINO3.4 and Western V SST to ENSO and West Pacific Warming Mode Empirical Orthogonal Functions (EOF). **A.** 1981-2022 correlation between the 1st Principal Component (PC) of tropical Pacific MAM SSTs and observed MAM SSTs. Yellow box denotes the NINO3.4 region. **B**. Same but for the WPWM and Western V region. **C**. Time-series of MAM WPWM and ENSO MAM PCs, expressed as standardized anomalies centered on a 1981-2021 baseline. **D**. Same for regional SST averaged over the Western V and NINO3.4.

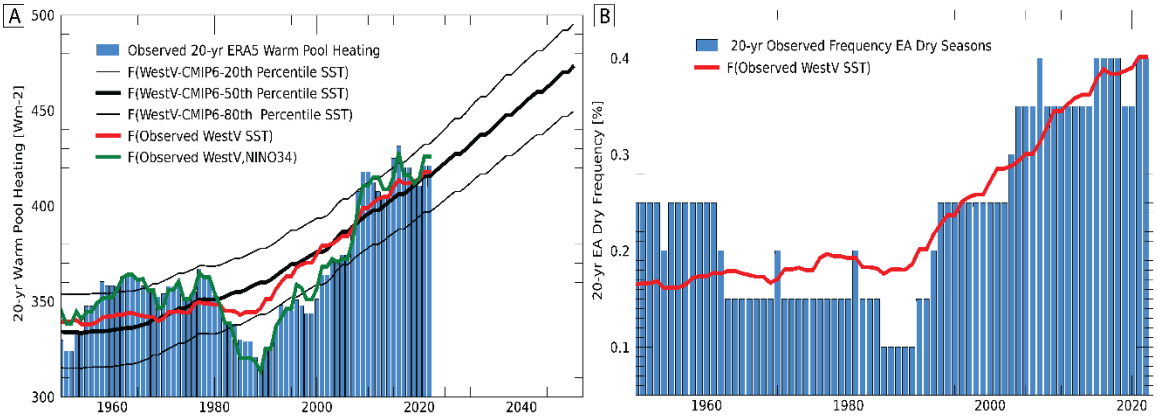

Figure 9. Relating Warm Pool heating and more frequent droughts to anthropogenic warming in the Western V. **A.** Observed and estimated 20-yr ERA5 West Pacific Heating V SST anomalies. The green line show regression estimates based on observed standardized 20-yr Western V and NINO3.4 SST. The red line shows estimates based only observed Western V. The thick black line shows 20-yr Warm Pool heating based on the median CMIP6 Western V SST estimates. The thin black lines show the spread of CMIP6 Warm Pool Heating estimates. **B**. The 20-yr observed frequency of EA dry seasons (i.e. circles in Figure 2C), along with Western V and NINO3.4-based regression estimates.

References

Adler, R. F., G. Gu, M. Sapiano, J.-J. Wang, and G. J. Huffman (2017), Global precipitation: Means, variations and trends during the satellite era (1979–2014), Surveys in Geophysics, 38(4), 679-699.

Bjerknes, J. (1969), Atmospheric teleconnections from the equatorial Pacific, Monthly Weather Review, 97(3), 163-172, doi: 10.1175/1520-0493(1969)097<0163:atftep>2.3.co;2.

Button, H. (2022), Famine Early Warning Systems Network forecasts alert USAID to impending food emergencies, edited, US Agency for International Development, Washington, DC.

Cai, W., B. Ng, G. Wang, A. Santoso, L. Wu, and K. Yang (2022), Increased ENSO sea surface temperature variability under four IPCC emission scenarios, Nature Climate Change, 12(3), 228-231, doi: 10.1038/s41558-022-01282-z.

Cai, W., A. Santoso, G. Wang, S.-W. Yeh, S.-I. An, K. M. Cobb, M. Collins, E. Guilyardi, F.-F. Jin, and J.-S. Kug (2015a), ENSO and greenhouse warming, Nature Climate Change.

Cai, W., G. Wang, A. Santoso, M. J. McPhaden, L. Wu, F.-F. Jin, A. Timmermann, M. Collins, G. Vecchi, and M. Lengaigne (2015b), Increased frequency of extreme La Niña events under greenhouse warming, Nature Climate Change, 5(2), 132-137.

Checchi, F., and W. C. Robinson (2013), Mortality among populations of southern and central Somalia affected by severe food insecurity and famine during 2010-2012*Rep.*, 87 pp, http://www.fsnau.org/downloads/Somalia_Mortality_Estimates_Final_Report_8May2013_upload.pdf, Rome, Washington.

1067 Dinku, T., C. Funk, P. Peterson, R. Maidment, T. Tadesse, H. Gadain, and P. Ceccato (2018),
1068 Validation of the CHIRPS satellite rainfall estimates over eastern of Africa, Quarterly
1069 Journal of the Royal Meteorological Society.
1070 Endris, H. S., C. Lennard, B. Hewitson, A. Dosio, G. Nikulin, and H.-J. Panitz (2016),
1071 Teleconnection responses in multi-GCM driven CORDEX RCMs over Eastern Africa,
1072 Climate Dynamics, 46(9), 2821-2846.
1073 Endris, H. S., C. Lennard, B. Hewitson, A. Dosio, G. Nikulin, and G. A. Artan (2019), Future
1074 changes in rainfall associated with ENSO, IOD and changes in the mean state over Eastern
1075 Africa, Climate dynamics, 52(3), 2029-2053.
1076 Endris, H. S., P. Omondi, S. Jain, C. Lennard, B. Hewitson, L. Chang'a, J. Awange, A. Dosio, P.
1077 Ketiem, and G. Nikulin (2013), Assessment of the performance of CORDEX regional
1078 climate models in simulating East African rainfall, Journal of Climate, 26(21), 8453-8475.
1079 Eyring, V., S. Bony, G. A. Meehl, C. A. Senior, B. Stevens, R. J. Stouffer, and K. E. Taylor
1080 (2016), Overview of the Coupled Model Intercomparison Project Phase 6 (CMIP6)
1081 experimental design and organization, Geoscientific Model Development, 9(5), 1937-1958.
1082 Finney, D. L., J. H. Marsham, D. P. Walker, C. E. Birch, B. J. Woodhams, L. S. Jackson, and S.
1083 Hardy (2020), The effect of westerlies on East African rainfall and the associated role of
1084 tropical cyclones and the Madden–Julian Oscillation, Quarterly Journal of the Royal
1085 Meteorological Society, 146(727), 647-664, doi: https://doi.org/10.1002/qj.3698.
1086 Funk, C., and A. Hoell (2015), The leading mode of observed and CMIP5 ENSO-residual sea
1087 surface temperatures and associated changes in Indo-Pacific climate, Journal of Climate,
1088 28(11), 4309-4329.
1089 Funk, C., and A. Hoell (2017), Recent Climate Extremes Associated with the West Pacific
1090 Warming Mode, in Climate Extremes: Patterns and Mechanisms, edited by S. Y. Wang, Jin-
1091 Ho; Funk, Chris; Gillies, Robert, Wiley Press, American Geophysical Union.
1092 Funk, C., and e. al. (2019), Recognizing the Famine Early Warning Systems Network (FEWS
1093 NET): Over 30 Years of Drought Early Warning Science Advances and Partnerships
1094 Promoting Global Food Security, Bull. Amer. Meteor. Soc. 100(6), 1010-1027.
1095 Funk, C., S. E. Nicholson, M. Landsfeld, D. Klotter, P. Peterson, and L. Harrison (2015a), The
1096 Centennial Trends Greater Horn of Africa precipitation dataset, Scientific Data, 2(150050),
1097 doi: 10.1038/sdata.2015.50.
1098 Funk, C., M. D. Dettinger, J. C. Michaelsen, J. P. Verdin, M. E. Brown, M. Barlow, and A. Hoell
1099 (2008), Warming of the Indian Ocean threatens eastern and southern African food security
1100 but could be mitigated by agricultural development, Proc Nat Acad Sci USA, 105(31),
1101 11081-11086.
1102 Funk , C., A. Hoell, S. Shukla, I. Bladé, B. Liebmann, J. B. Roberts, and G. Husak (2014),
1103 Predicting East African spring droughts using Pacific and Indian Ocean sea surface
1104 temperature indices, Hydrology and Earth System Sciences Discussions, 11(3), 3111-3136.
1105 Funk, C., G. Senay, A. Asfaw, J. Verdin, J. Rowland, J. Michaelson, G. Eilerts, D. Korecha, and
1106 R. Choularton (2005), Recent drought tendencies in Ethiopia and equatorial-subtropical
1107 eastern Africa, *Vulnerability to Food Insecurity: Factor Identification and Characterization*
1108 *Report, 1*, 12.
1109 Funk, C., P. Peterson, M. Landsfeld, D. Pedreros, J. Verdin, S. Shukla, G. Husak, J. Rowland, L.
1110 Harrison, and A. Hoell (2015b), The climate hazards infrared precipitation with stations—a
1111 new environmental record for monitoring extremes, Scientific data, 2.

1112 Funk, C., et al. (2018), Examining the role of unusually warm Indo-Pacific sea surface
1113 temperatures in recent African droughts Quart J Roy Meteor Soc, 144, 360-383, doi:
1114 10.1002/qj.3266.
1115 Funk, C., et al. (2019), Examining the potential contributions of extreme 'Western V' sea surface
1116 temperatures to the 2017 March-June East African Drought, Bull. Amer. Meteor. Soc.,
1117 100(1), S55-S60.
1118 Gelaro, R., et al. (2017), The Modern-Era Retrospective Analysis for Research and Applications,
1119 Version 2 (MERRA-2), Journal of Climate, 30(14), 5419-5454, doi: 10.1175/JCLI-D-16-
1120 0758.1.
1121 Gill, A. E. (1980), Some simple solutions for heat-induced tropical circulation, Q J Roy Meteor
1122 Soc, 106, 447-462.
1123 Gill, A. E. (1982), Atmosphere-ocean dynamics, 662 pp., Academic Press, San Diego.
1124 Gudoshava, M., H. O. Misiani, Z. T. Segele, S. Jain, J. O. Ouma, G. Otieno, R. Anyah, V. S.
1125 Indasi, H. S. Endris, and S. Osima (2020), Projected effects of 1.5 C and 2 C global warming
1126 levels on the intra-seasonal rainfall characteristics over the Greater Horn of Africa, Environ
1127 Res Lett, 15(3), 034037.
1128 Hersbach, H., B. Bell, P. Berrisford, S. Hirahara, A. Horányi, J. Muñoz-Sabater, J. Nicolas, C.
1129 Peubey, R. Radu, and D. Schepers (2020), The ERA5 global reanalysis, Quarterly Journal of
1130 the Royal Meteorological Society, 146(730), 1999-2049.
1131 Hoell, A., and C. Funk (2013a), Indo-Pacific sea surface temperature influences on failed
1132 consecutive rainy seasons over eastern Africa, Climate Dynamics, 43(5-6), 1645-1660.
1133 Hoell, A., and C. Funk (2013b), The ENSO-Related West Pacific Sea Surface Temperature
1134 Gradient, Journal of Climate, 26(23), 9545-9562.
1135 Huang, B., P. W. Thorne, V. F. Banzon, T. Boyer, G. Chepurin, J. H. Lawrimore, M. J. Menne,
1136 T. M. Smith, R. S. Vose, and H.-M. Zhang (2017), Extended Reconstructed Sea Surface
1137 Temperature, Version 5 (ERSSTv5): Upgrades, Validations, and Intercomparisons, Journal
1138 of Climate, 30(20), 8179-8205, doi: 10.1175/JCLI-D-16-0836.1.
1139 Husak, G. J., J. Michaelsen, and C. Funk (2007), Use of the gamma distribution to represent
1140 monthly rainfall in Africa for drought monitoring applications, International Journal of
1141 Climatology, 27(7), 935-944.
1142 ICPAC, FEWS-NET, WMO, FAO, WFP, and JRC (2022a), Unprecedented drought brings threat
1143 of starvation to millions in Ethiopia, Kenya, and Somalia, *Multi-Agency Drought Alert*.
1144 ICPAC, et al. (2022b), Immediate global action required to prevent Famine in the Horn of
1145 Africa, *Multi-agency Drought Alert*.
1146 Johnson, N. C. (2013), How many ENSO flavors can we distinguish?, Journal of Climate,
1147 26(13), 4816-4827.
1148 Kilavi, M., D. MacLeod, M. Ambani, J. Robbins, R. Dankers, R. Graham, H. Titley, A. A. Salih,
1149 and M. C. Todd (2018), Extreme rainfall and flooding over central Kenya including Nairobi
1150 city during the long-rains season 2018: causes, predictability, and potential for early warning
1151 and actions, Atmosphere, 9(12), 472.
1152 Kirtman, B. P., D. Min, J. M. Infanti, J. L. Kinter III, D. A. Paolino, Q. Zhang, H. van den Dool,
1153 S. Saha, M. P. Mendez, and E. Becker (2014), The North American Multimodel Ensemble:
1154 Phase-1 seasonal-to-interannual prediction; phase-2 toward developing intraseasonal
1155 prediction, B Am Meteorol Soc, 95(4), 585-601.

L'Heureux, M. L., S. Lee, and B. Lyon (2013), Recent multidecadal strengthening of the Walker circulation across the tropical Pacific, Nature Climate Change, 3(6), 571-576, doi: doi:10.1038/nclimate1840.

Liebmann, B., I. Bladé, G. N. Kiladis, L. M. Carvalho, G. B. Senay, D. Allured, S. Leroux, and C. Funk (2012), Seasonality of African precipitation from 1996 to 2009, Journal of Climate, 25(12), 4304-4322.

Liebmann, B., M. P. Hoerling, C. Funk , I. Bladé, R. M. Dole, D. Allured, X. Quan, P. Pegion, and J. K. Eischeid (2014), Understanding Recent Eastern Horn of Africa Rainfall Variability and Change, J. Climate, 27(23), 8630-8645.

Lyon, B. (2014), Seasonal Drought in the Greater Horn of Africa and its Recent Increase During the March-May Long Rains, Journal of Climate, 27(2014), 7953-7975.

Lyon, B. (2020), Biases in CMIP5 Sea Surface Temperature and the Annual Cycle of East African Rainfall, Journal of Climate, 33(19), 8209-8223.

Lyon, B. (2021), Biases in sea surface temperature and the annual cycle of Greater Horn of Africa rainfall in CMIP6, International Journal of Climatology.

Lyon, B., and D. G. DeWitt (2012), A recent and abrupt decline in the East African long rains, GEOPHYSICAL RESEARCH LETTERS, 39(L02702).

Lyon, B., and N. Vigaud (2017), Unraveling East Africa's climate paradox, Climate extremes: Patterns and mechanisms, 265, 281.

Lyon, B., A. G. Barnston, and D. G. DeWitt (2013), Tropical pacific forcing of a 1998–1999 climate shift: observational analysis and climate model results for the boreal spring season, Climate Dynamics, 43 (3-4), 893-909.

MacLeod, D. (2018), Seasonal predictability of onset and cessation of the east African rains, Weather and climate extremes, 21, 27-35.

Mantua, N., and S. Hare (2002), The Pacific Decadal Oscillation, Journal of Oceanography, 58(1), 35-44, doi: 10.1023/a:1015820616384.

Meinshausen, M., Z. R. Nicholls, J. Lewis, M. J. Gidden, E. Vogel, M. Freund, U. Beyerle, C. Gessner, A. Nauels, and N. Bauer (2020), The shared socio-economic pathway (SSP) greenhouse gas concentrations and their extensions to 2500, Geoscientific Model Development, 13(8), 3571-3605.

Nicholson, S. E. (2015), Long-term variability of the East African 'short rains' and its links to large-scale factors, International Journal of Climatology, n/a-n/a, doi: 10.1002/joc.4259.

Nicholson, S. E. (2017), Climate and Climatic Variability of Rainfall over Eastern Africa, Reviews of Geophysics, n/a-n/a, doi: 10.1002/2016RG000544.

NOAA (2022), Cold & Warm Episodes by Season, edited by C. P. Center.

Ogega, O. M., J. Koske, J. B. Kung'u, E. Scoccimarro, H. S. Endris, and M. N. Mistry (2020), Heavy precipitation events over East Africa in a changing climate: results from CORDEX RCMs, Climate Dynamics, 55(3), 993-1009.

Park, S., D. Kang, C. Yoo, J. Im, and M.-I. Lee (2020), Recent ENSO influence on East African drought during rainy seasons through the synergistic use of satellite and reanalysis data, ISPRS Journal of Photogrammetry and Remote Sensing, 162, 17-26.

Peixoto, J. P., and A. H. Oort (1992), Physics of Climate, Am. Inst. Physics, New York.

Rowell, D. P., B. B. B. Booth, S. E. Nicholson, and P. Good (2015), Reconciling Past and Future Rainfall Trends over East Africa, Journal of Climate, 28(24), 9768-9788, doi: 10.1175/JCLI-D-15-0140.1.

Roxy, M. K., P. Dasgupta, M. J. McPhaden, T. Suematsu, C. Zhang, and D. Kim (2019), Twofold expansion of the Indo-Pacific warm pool warps the MJO life cycle, Nature, 575(7784), 647-651, doi: 10.1038/s41586-019-1764-4.

Rubiano, M. P. (2022), How Scientists Predict Famine Before It Hits, *BBC Future Planet*.

Schwarzwald, K., L. Goddard, R. Seager, M. Ting, and K. Marvel (2022), Understanding CMIP6 Biases in the Representation of the Greater Horn of Africa Long and Short Rains.

Seager, R., N. Henderson, and M. Cane (2022), Persistent discrepancies between observed and modeled trends in the tropical Pacific Ocean, Journal of Climate, 1-41, doi: 10.1175/jcli-d-21-0648.1.

Seager, R., M. Cane, N. Henderson, D.-E. Lee, R. Abernathey, and H. Zhang (2019), Strengthening tropical Pacific zonal sea surface temperature gradient consistent with rising greenhouse gases, Nature Climate Change, 9(7), 517-522, doi: 10.1038/s41558-019-0505-x.

Shukla, S., J. Roberts, A. Hoell, C. C. Funk, F. Robertson, and B. Kirtman (2016), Assessing North American multimodel ensemble (NMME) seasonal forecast skill to assist in the early warning of anomalous hydrometeorological events over East Africa, Climate Dynamics, 1-17, doi: 10.1007/s00382-016-3296-z.

Shukla, S., G. Husak, W. Turner, F. Davenport, C. Funk, L. Harrison, and N. Krell (2021), A slow rainy season onset is a reliable harbinger of drought in most food insecure regions in Sub-Saharan Africa, Plos one, 16(1), e0242883.

Tierney, J., J. Smerdon, K. Anchukaitis, and R. Seager (2013), Multidecadal variability in East African hydroclimate controlled by the Indian Ocean, Nature, 493(7342), 389-392.

Tierney, J. E., C. C. Ummenhofer, and P. B. deMenocal (2015), Past and future rainfall in the Horn of Africa, Science Advances, 1(9), 1-8, doi: 10.1126/sciadv.1500682.

Trenberth, K. E., and D. P. Stepaniak (2003a), Covariability of components of poleward atmospheric energy transports on seasonal and interannual timescales, Journal of Climate, 16(22), 3691-3705.

Trenberth, K. E., and D. P. Stepaniak (2003b), Seamless poleward atmospheric energy transports and implications for the Hadley circulation, Journal of Climate, 16(22), 3706-3722.

Verdin, J., C. Funk, G. Senay, and R. Choularton (2005), Climate science and famine early warning, Philos T Roy Soc B, 360(1463), 2155-2168.

Voosen, P. (2020), The hunger forecast, Science, 368(6488), 226-229, doi: DOI: 10.1126/science.368.6488.226.

Wainwright, C. M., J. H. Marsham, R. J. Keane, D. P. Rowell, D. L. Finney, E. Black, and R. P. Allan (2019), 'Eastern African Paradox'rainfall decline due to shorter not less intense Long Rains, npj Climate and Atmospheric Science, 2(1), 1-9.

Walker, D. P., J. H. Marsham, C. E. Birch, A. A. Scaife, and D. L. Finney (2020), Common Mechanism for Interannual and Decadal Variability in the East African Long Rains, Geophysical Research Letters, 47(22), e2020GL089182, doi: https://doi.org/10.1029/2020GL089182.

Williams, P., and C. Funk (2011), A westward extension of the warm pool leads to a westward extension of the Walker circulation, drying eastern Africa, Climate Dynamics, 37(11-12), 2417-2435.

Wills, R. C. J., Y. Dong, C. Proistosecu, K. C. Armour, and D. S. Battisti (2022), Systematic Climate Model Biases in the Large-Scale Patterns of Recent Sea-Surface Temperature and Sea-Level Pressure Change, Geophysical Research Letters, 49(17), e2022GL100011, doi: https://doi.org/10.1029/2022GL100011.

1247 Yang, W., R. Seager, M. A. Cane, and B. Lyon (2014), The East African Long Rains in
1248 Observations and Models, Journal of Climate, 27(19), 7185-7202, doi: 10.1175/JCLI-D-13-
1249 00447.1.
1250